MASDOC Research Study Group Report: A Model of Metal Ring Rolling

Dominic Brockington Trishen Gunaratnam Christian Scharrer

April 16, 2018

1 Introduction

In metal industry, after ore extraction, smelting, and casting, the last stage of metal production is the forming, where one shapes the metal workpiece by mechanical means. In other words, metal formation processes are used in order to shape a metal workpiece into a final product. Typically, at this stage, the steel will be rolled. We considered such a roll process where the metal comes as a ring. This is used to create a seamless, jointless, and smooth metal ring of desired size and achieved by repeatedly passing the annealing ring between two vertical rolls which thin the ring. Horizontal, conical rolls limit height growth and vertical guide rolls are used to keep the ring stable. The final result is a thinner ring of greater radius. An example of this setup is shown in figure 1.

Figure 1: Ring rolling diagram, taken from [Min17], Section 1.2

Although ring rolling is used a lot in industry, e.g. for oil platform legs or aircraft engine parts, a flexible and accurate analytical model does not exist. Approaches to achieve an analytical model in 2D (ignoring the conical and guide rolls) in the past have had strict assumptions on the circularity, coaxality, and centrality of the ring. Respectively, these measure how close the ring remains to a circle in shape, how uniform the thickness of the ring is, and how centred the ring remains to the line of symmetry of the rollers. See for instance: [HJKA73] and [PA14], which focus on the roll gap only; [PAS11], [AAA16], [RDS17] which focus on slab models; and we also highlight mass conservation models proposed in [BQM15] and [GY11]. Current developments in industry have been concerned with controlling the resulting shape of the ring: attempting to create elliptical

or polygonal rings, and trying to produce rings with non-rectangular cross sections, such as an L shape (see [TIST05], [KMK90], and [YKKL03]). As such, a model of ring rolling which is flexible with regards to circularity, coaxiality and centrality is desired; not only that it could lead to more automation, it may also lead to better metal forming of other geometries, saving a lot of energy and material.

The approach laid out in [Min17] by Minton is a convincing step forward to a flexible analytical model. The idea is to split the problem into an inner model of the roll gap region, which is analysed by slab methods, see 4, and a curved beam outer model of the outer region of the ring, see 3. Then, one is aiming for a coupling of the two models by force and geometry. Accordingly, Minton's work is considered to be incomplete since he couldn't achieve satisfying results of the coupling. Moreover, Minton's chapter on Ring Rolling, Chapter 6 in [Min17] is not self-contained. In fact, details about how to derive the differential equations of the inner model are not provided in [Min17]. Nevertheless, we believe that this approach is a good foundation for future investigations of developing a flexible theory of ring rolling. As our contribution, we tried to verify Minton's model in two ways. First, with slight modifications, we re-derived the differential equations of the the inner model. In this report, we shall give detailed explanation and full mathematical derivation of both, the inner model and the outer model. Secondly, we implemented the inner and the outer model numerically in MATLAB, tested the code against various data-sets and analysed the results, see Chapter 5. Finally, as an outlook, we shall give detailed explanation about our ideas how to couple the two models, see Chapter 6.

Acknowledgements

We would like to thank our supervisors Ed Brambley and Andreas Dedner for their encouragement and helpful discussion. We would also like to thank the University of Warwick and EPSRC for funding our research.

2 Preliminaries

In this section, we provide basic definitions and notation for the dynamics and kinematics of *simple bodies*, that is, for open subsets B in $\mathbf{R}^3$, within the framework of continuum mechanics. While the physics governing the outer model is elasticity theory and the physics governing the inner model is plasticity theory, both, elasticity and plasticity are based on a particular mutual dependency of stress and strain. We start by introducing the strain tensor and the stress tensor. Then, we describe their particular dependency in elasticity and plasticity. Moreover, we will state Castigliano's theorem, which is the basic tool of the outer model.

2.1 The Strain Tensor

For the content of this section, see [MH94, Section 1.1] and [Lub08, Section 1.2]. A *configuration* of a simple body $B \subset \mathbf{R}^3$ is a continuous map $\phi : B \to \mathbf{R}^3$. For any such configuration, the map $u : B \to \mathbf{R}^3$ given by

$$u(x) = \phi(x) - x, \quad \text{for } x \in B$$

is called *displacement*. The symmetric part of the space derivative of u,

$$\varepsilon = \frac{1}{2}(\mathrm{D}u + (\mathrm{D}u)^*)$$

is called *strain tensor*, where $(\mathrm{D}u)^*$ is the adjoint associated to $\mathrm{D}u$. The stress tensor ε is related to the deformation of the transformed body $\phi[B]$ compared with its initial configuration B. The components are given by

$$\varepsilon_{ij} = \frac{1}{2}\left(\partial_{x_i} u_j + \partial_{x_j} u_i\right).$$

Notice, that u, as well as the following quantities, can be considered time dependent, since ϕ can be realised a point on a curve in the space of all configurations of B. Such a curve $t \mapsto \phi_t$ is called *motion* of B.

2.2 The Stress Tensor

For the content of this section, see [MH94, Section 2.2] and [Lub08, Section 1.3]. Suppose ϕ describes the motion of a simple body $B \subset \mathbf{R}^3$. At each time t, the forces acting on $\phi_t[B]$ can be divided into long range forces, given by a vector field $\mathbf{b}$, and short range forces, given by $\mathbf{t}$. The short range forces exerted on a body are felt on its surface. That means, any oriented surface element $d\mathbf{S} = \mathbf{n}dS$ experiences a contact force $\mathbf{t}(\mathbf{n})dS$, where $\mathbf{n}$ the outward unit normal. Therefore, the so called *surface traction* $\mathbf{t}(\mathbf{n})$ not only depends on position but also on the local orientation and hence is not a vector field. We henceforth assume that *balance of linear momentum* is satisfied. That is,

$$\frac{d}{dt}\int_{\phi_t[U]} \rho\mathbf{v}\, dV = \int_{\phi_t[U]} \rho\mathbf{b}\, dV + \int_{\partial\phi_t[U]} \mathbf{t}\, dS$$

for each time t and all sufficiently regular open subsets U of B, where ρ is the mass density function and $\mathbf{v}$ is the spatial velocity. Standard arguments due to Cauchy, employing the Cauchy tetrahedron, show that $\mathbf{t}(\cdot)$ is a linear function. Hence, there exists a $(2,0)$ tensor field $\boldsymbol{\sigma}$, satisfying

$$\mathbf{t}(x,t,\mathbf{n}) = \boldsymbol{\sigma}(x,t)\mathbf{n} \quad \text{for each time } t \text{ and } x \in \phi_t[B],$$

called *stress tensor*. Moreover, we will assume that *balance of angular momentum* is satisfied. That is

$$\frac{d}{dt}\int_{\phi_t[U]} \rho x \times \mathbf{v}\, dV = \int_{\phi_t[U]} \rho x \times \mathbf{b}\, dV + \int_{\partial\phi_t[U]} x \times \sigma\mathbf{n}\, dS$$

for all $x \in \mathbf{R}^3$, each time t, and all sufficiently regular open subsets U of B. Using Gauss's theorem, one can show

$$\sigma_{ij} = \sigma_{ji}.$$

In other words, the stress tensor is symmetric.

We define the components s_{ij} of the *deviatoric stress* tensor $\mathbf{s}$ by

$$s_{ij} = \sigma_{ij} - p\delta_{ij}$$

where δ_{ij} is the Kronecker delta and $p = \sum_{k=1}^{3} \sigma_{kk}$ is the pressure.

We will be concerned with the 2-dimensional simplification in which case we shall use the following notation for the stress components:

$$\boldsymbol{\sigma} = \begin{pmatrix} \sigma_x & \tau \\ \tau & \sigma_y \end{pmatrix}.$$

2.3 Elasticity and Castigliano's Theorem

For the content of this section, see [Lub08, Section 1.4] and [Sha64, Chapter 10]. A region of a body is called elastic if no permanent deformation occurs. In so called *linear elasticity*, this means the generalised Hooke's law is satisfied. That is, there exists a constant $(4,0)$ tensor with components C_{ijkl}, called *elastic constants*, such that in the relevant region

$$\sigma_{ij} = \sum_{k,l=1}^{3} C_{ijkl}\varepsilon_{kl}.$$

In other words, the stress is proportional to the strain. Most metallic alloys are considered *isotropic*, where by definition the material properties are independent of direction, or mathematically expressed,

$$C_{ijkl} = \lambda\delta_{ij}\delta_{kl} + \mu(\delta_{ik}\delta_{jl} + \delta_{il}\delta_{jk})$$

for some constants λ and μ called *Lamé coefficients*. One defines *Young's modulus* $E = \mu(3\lambda + 2\mu)/(\lambda + \mu)$ and the shear modulus $G = \mu$.

While a system undergoes deformation, it will store energy. We define the strain energy function $W(\varepsilon)$ and the strain energy U of a body B by

$$\sigma_{ij} = \frac{\partial W}{\partial \varepsilon_{ij}}, \qquad U = \int_B W \, dV.$$

We will be concerned with the case that the strain energy of a linear elastic body is given by the work done by a force f. More precisely, we assume that the strain energy can be expressed as a function of a force f. In this case, Castigliano's theorem states that the general displacement δx of the point of force application in direction of the force f is given by the partial derivative of the strain energy with respect to f. That means, we have the equation

$$\frac{\partial U}{\partial f} = \delta x.$$

See also [TG51, 49].

2.4 Plasticity Theory

In elastic deformations, the strain tensor can be thought of as only a function of the stress and the temperature T. Plasticity is when the strain additionally depends on internal variables, ξ. Internal variables could represent material properties or the history of the strain, as well as stress and temperature. We make the ansatz that the strain tensor splits into elastic and inelastic parts: $\varepsilon(\sigma, T, \xi) = \varepsilon^e(\sigma, T) + \varepsilon^i(\xi)$.

Viscoplasticity is a model of plasticity that assumes the existence of a continuous yield function $f = f(\sigma, T, \xi)$ and a region R of the σ, T, ξ- space such that: $f < 0$ and $\partial_t \varepsilon^i = 0$ inside R but not outside it. Such a region is called the elastic region. The boundary, $f = 0$, is called the yield surface. The physics behind this is that whilst we are within R only elastic deformation occurs but once we reach the yield surface, plastic deformation occurs. Rigid perfect plasticity is when no elastic deformation occurs.

We will be concerned with a 2D problem and we shall use the von-Mises yield function,

$$f(\sigma, \xi) = \left(\frac{\sigma_x - \sigma_y}{2} \right)^2 + \tau^2 - k(\xi)^2, \tag{1}$$

where σ_x, σ_y, and τ are the components of the stress tensor, and k is parameter intrinsic to the material that can be determined experimentally. We remark that the nature of the yield function (1) suggests that the yield surface is elliptical: this is in line with experimental data on yield surfaces of metals, and is evidence that this is the right yield function to use in modelling ring rolling.

3 Outer Model

In this section we shall describe the outer section of the beam, and explain our model. The outer section of the beam undergoes forces that are considerably smaller than those acting on the beam between the rolls, and we consider all deformation to be elastic. We have a curved beam undergoing elastic deformation, we recall Castigliano's theorem

$$\frac{\partial U}{\partial f_x} = \delta x \tag{2}$$

where U is the strain energy of the solid, f_x the force acting on it in some direction x, and δx the displacement in the same direction x.

We can use the following formula, derived by Timoshenko (1925) [Tim25], for the strain energy of a curved beam

$$U = \int_\Gamma \frac{M^2}{RA\gamma E} - \frac{MS}{AER} + \frac{S^2}{2AE} + \frac{\kappa Q^2}{AG} ds \tag{3}$$

where M is the local bending moment around the centreline, S the longitudinal force, and Q the shear force.

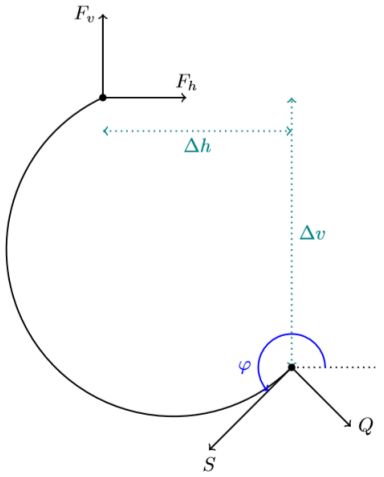

Figure 2: Variables in the outer model

- Γ is the centreline of the beam,
- A the area of the cross section of the beam (assumed to be rectangular),
- R the radius of curvature
- γ is the distance between the centreline and the neutral axis, this is calculated using a series formula given in Timoshenko [Tim25].
- κ is a numerical factor accounting for the distance between the neutral and centre axes, in this case it is taken as 1.5;
- E and G are the Young's and shear moduli respectively.

It should be noted that γ is no larger than the width of the beam, in fact it is relatively small and thus the first term in the integral is dominant. To find M, S, and Q we assume a force and moment balance on each part of the beam; this is justified by the small accelerations each segment undergoes. Using the notation and conventions given in the figure this gives the following equalities

$$\begin{aligned} S &= -F_v \sin(\phi) + F_h \cos(\phi) \\ Q &= -F_v \cos(\phi) - F_h \sin(\phi) \\ M &= -M_0 + F_v \Delta h - F_h \Delta v. \end{aligned}$$

Here M and M_0 are the moments around the centreline, and are taken anti-clockwise. Putting these formulae into equation (3) and taking partial derivatives with respect to F_h, F_v, and M_0 gives the horizontal, vertical and angular displacements respectively between the two ends of the beam

$$\begin{aligned} \delta x &= \int_\Gamma \Delta v\Big(\frac{S}{AER} - \frac{M}{RA\gamma E}\Big) + \cos(\phi)\Big(\frac{S}{AE} - \frac{M}{AER}\Big) - \sin(\phi)\frac{\kappa Q}{AG} ds \\ \delta y &= \int_\Gamma \Delta h\Big(\frac{M}{RA\gamma E} - \frac{S}{AER}\Big) + \sin(\phi)\Big(\frac{M}{AER} - \frac{S}{AE}\Big) - \cos(\phi)\frac{\kappa Q}{AG} ds \\ \delta\theta &= \int_\Gamma \frac{S}{AER} - \frac{M}{RA\gamma E} ds. \end{aligned}$$

In addition, we can find Δh and Δv if we have Γ parametrised with respect to ϕ and the distance from some fixed point, r, as

$$\begin{aligned} \Delta h &= r_0 \sin(\phi_0) - r \sin(\phi) \\ \Delta v &= r_0 \cos(\phi_0) - r \cos(\phi). \end{aligned}$$

Where r_0 is the initial value of r in the parametrisation of Γ at the point where the beam enters the roll gap, and ϕ_0 is the corresponding value of ϕ. These integrals can then be calculated if Γ, A, and the initial forces are known. This was done for a circular beam. Some results, including error analysis are displayed below. The code itself will be discussed later in the report.

The left plot of figure 3 shows the deformation of a circular beam under a variety of forces, displaying intuitively correct behaviour.

The right plot of figure 3 shows the difference between the work done by the forces acting on the end of the beam and the strain energy calculated by the Timoshenko equation, plotted against the step size used in the integration. This was done for a fixed set of initial forces and ring geometry. It shows the error is linearly related to the step size, whilst the error may seem large in the beginning it should be noted that the work and strain energy calculated are considerably larger, and so the relative difference is quite small. This provides some validity for the model.

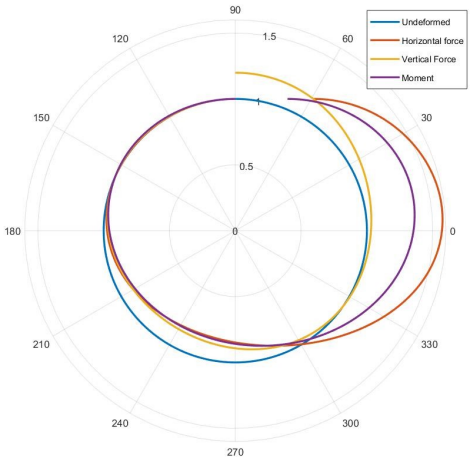

(a) Example deformations of a circular beam

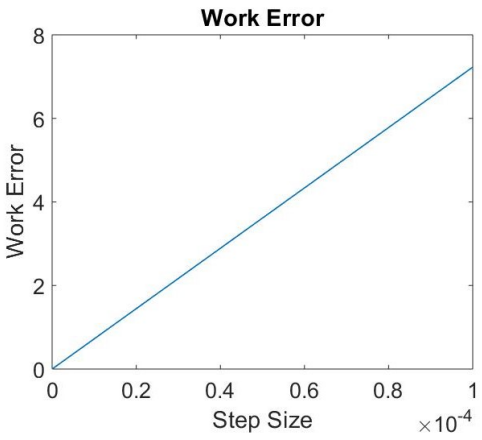

(b) Energy Comparison for the outer model

Figure 3: Outer model

4 Inner Model

In this section, we analyse the inner model via an extended slab method as in [Min17], Section 6. First we set up the geometry of the model. Then, based on a force and moment balance, we derive three differential equations. Finally, by assuming linear variation of the horizontal stress through thickness across the roll gap, using a friction law, and using yield conditions, we turn the differential equations into a closed system of ordinary differential equations.

4.1 Set-up

We fix our reference picture of the model as Figure 4.

- x_t^{in} and x_b^{in} mark the entry contact points for the top and bottom roll respectively; x_t^{out} and x_b^{out} mark the exit contact points for the top and bottom roll respectively.
- x_t^n and x_b^n refer to the neutral points on the top and bottom roll respectively: these are points at which the direction of friction changes, so that material is pushed towards neutral points. We emphasise that the rolling model does not require these neutral points to coincide vertically.
- $h_t(x)$ and $h_b(x)$ parametrize the top and the bottom roll respectively.
- R_t and R_b denote the radii of the top and the bottom roll respectively.
- w_0 denotes the distance of minimal separation of the two rolls.

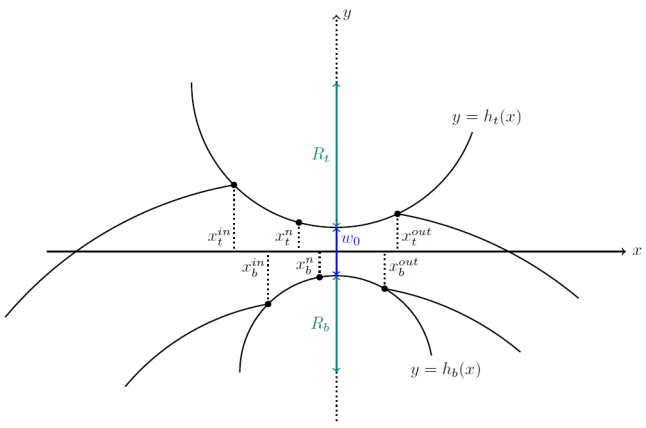

Figure 4: Diagram of the Inner Model

4.2 Analysis Via the Slab Method

We consider small vertical strips of the ring of width δx between the two rolls. We model the top and the bottom surface of each such wedge as a line segment rather than a circle segment. This approximation will not effect our calculations and the ODEs derived with the slab model will be accurate. The slab model is based on a force and torque balance around each slab. To determine torque and forces, we introduce the following notation and convention according to Figure 5.

- The components of the stress tensor

$$\boldsymbol{\sigma} = \begin{pmatrix} \sigma_x & \tau \\ \tau & \sigma_y \end{pmatrix}$$

  are functions of x and y on the ring.

- The normal vector $\mathbf{n}$ and the tangential vector $\mathbf{t}$ at the top of the wedge are given by

$$\mathbf{n} = \frac{-h_t' \mathbf{e}_x + \mathbf{e}_y}{\sqrt{1 + h_t'^2}}, \qquad \mathbf{t} = \frac{\mathbf{e}_x + h_t' \mathbf{e}_y}{\sqrt{1 + h_t'^2}},$$

- The normal vector $\mathbf{n}$ and the tangential vector $\mathbf{t}$ at the bottom of the wedge are given by

$$\mathbf{n} = \frac{h_b' \mathbf{e}_x - \mathbf{e}_y}{\sqrt{1 + h_b'^2}}, \qquad \mathbf{t} = \frac{\mathbf{e}_x + h_b' \mathbf{e}_y}{\sqrt{1 + h_b'^2}}.$$

- The normal vector $\mathbf{n}$ and the tangential vector $\mathbf{t}$ along the left vertical line of the wedge are given by

$$\mathbf{n} = -\mathbf{e}_x, \qquad \mathbf{t} = \mathbf{e}_y,$$

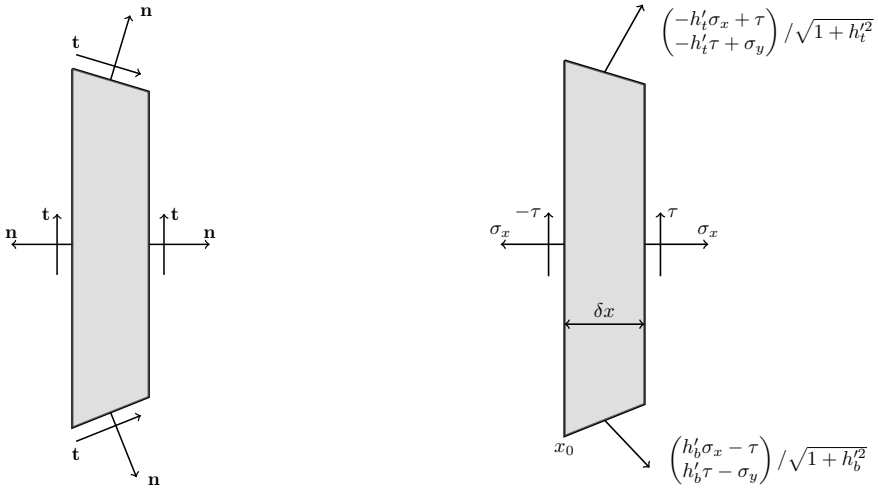

(a) Tangent and normal vectors

(b) Forces per unit length

Figure 5: Sign convention and forces per unit length

- The normal vector $\mathbf{n}$ and the tangential vector $\mathbf{t}$ at the bottom of the wedge are given by

$$\mathbf{n} = \mathbf{e}_x, \qquad \mathbf{t} = \mathbf{e}_y.$$

We get the forces per unit length at the top and the bottom of the wedge respectively, by calculating $\boldsymbol{\sigma}\mathbf{n}$ as

$$\begin{pmatrix} -h_t'\sigma_x + \tau \\ -h_t'\tau + \sigma_y \end{pmatrix} / \sqrt{1+h_t'^2} \quad \text{and} \quad \begin{pmatrix} h_b'\sigma_x - \tau \\ h_b'\tau - \sigma_y \end{pmatrix} / \sqrt{1+h_b'^2}.$$

Each force element per unit length $\boldsymbol{\sigma}\mathbf{n}$ splits as

$$\boldsymbol{\sigma}\mathbf{n} = \mathbf{t} \cdot (\boldsymbol{\sigma}\mathbf{n})\mathbf{t} + \mathbf{n} \cdot (\boldsymbol{\sigma}\mathbf{n})\mathbf{n}.$$

Along the left and the right vertical line segment we therefore get respectively for $\boldsymbol{\sigma}\mathbf{n}$

$$\sigma_x\mathbf{n} - \tau\mathbf{t} \quad \text{and} \quad \sigma_x\mathbf{n} + \tau\mathbf{t}.$$

Integrating the forces per unit length in direction of $\mathbf{e}_x$ along the boundary of a slab through x_0 and $x_0 + \delta$ and balance them gives

$$\begin{aligned} 0 = &\int_{h_b(x_0+\delta x)}^{h_t(x_0+\delta x)} \sigma_x(x_0+\delta x, y)\,\mathrm{d}y - \int_{h_b(x_0)}^{h_t(x_0)} \sigma_x(x_0, y)\,\mathrm{d}y \\ &+ \int_{x_0}^{x_0+\delta x} -h_t'(x)\sigma_x(x, h_t(x)) + \tau(x, h_t(x))\,\mathrm{d}x + \int_{x_0}^{x_0+\delta x} h_b'(x)\sigma_x(x, h_b(x)) - \tau(x, h_b(x))\,\mathrm{d}x. \end{aligned}$$

The first two terms equal

$$\begin{aligned}
&\int_{h_b(x_0)+h_b'(x_0)\delta x}^{h_t(x_0)+h_t'(x_0)\delta x} \sigma_x(x_0,y) + \delta x \frac{\partial \sigma_x}{\partial x}(x_0,y)\,\mathrm{d}y + \int_{h_b(x_0)}^{h_t(x_0)} \sigma_x(x_0,y)\,\mathrm{d}y + o(\delta x)\\
&= \left(\int_{h_t(x_0)}^{h_t(x_0)-h_t'(x_0)\delta x} + \int_{h_b(x_0)}^{h_b(x_0)+h_t'(x_0)\delta x}\right)\sigma_x(x_0,y)\,\mathrm{d}y + \delta x \int_{h_b(x_0)}^{h_t(x_0)} \frac{\partial \sigma_x}{\partial x}(x_0,y)\,\mathrm{d}y + o(\delta x)\\
&= h_t'(x_0)\delta x \sigma_x(x_0,h_t(x_0)) - h_b'(x_0)\delta x \sigma_x(x_0,h_b(x_0)) + \delta x \frac{\partial}{\partial x}\int_{h_b(x_0)}^{h_t(x_0)} \sigma_x(x_0,y)\,\mathrm{d}y\\
&\quad - \delta x[\sigma_x(x_0,h_t(x_0))h_t'(x_0) - \sigma_x(x_0,h_b(x_0))h_b'(x_0)] + o(\delta x).
\end{aligned}$$

Therefore, dividing the force balance equation by δx and letting $\delta x \to 0$ we have in the limit

$$\begin{aligned}
0 &= h_t'(x_0)\sigma_x(x_0,h_t(x_0)) - h_b'(x_0)\sigma_x(x_0,h_b(x_0)) + \frac{\partial}{\partial x}\int_{h_b(x_0)}^{h_t(x_0)} \sigma_x(x_0,y)\,\mathrm{d}y\\
&\quad + \sigma_x(x_0,h_b(x_0))h_b'(x_0) - \sigma_x(x_0,h_t(x_0))h_t'(x_0)\\
&\quad - h_t'(x_0)\sigma_x(x_0,h_t(x_0)) + \tau(x_0,h_t(x_0)) + h_b'(x_0)\sigma_x(x_0,h_b(x_0)) - \tau(x_0,h_b(x_0))\\
&= \frac{\partial}{\partial x}\int_{h_b(x_0)}^{h_t(x_0)} \sigma_x(x_0,y)\,\mathrm{d}y\\
&\qquad + h_b'(x_0)\sigma_x(x_0,h_b(x_0)) - h_t'(x_0)\sigma_x(x_0,h_t(x_0)) + \tau(x_0,h_t(x_0)) - \tau(x_0,h_b(x_0))
\end{aligned}$$

or shorter

$$\partial_x \int_{h_b}^{h_t} \sigma_x\,\mathrm{d}y = h_t'\sigma_x(h_t) - h_b'\sigma_x(h_b) + \tau(h_b) - \tau(h_t).$$

The vertical force balance in direction of $\mathbf{e}_y$ gives

$$\begin{aligned}
0 &= \int_{h_b(x_0+\delta x)}^{h_t(x_0+\delta x)} \tau(x_0+\delta x,y)\,\mathrm{d}y - \int_{h_b(x_0)}^{h_t(x_0)} \tau(x_0,y)\,\mathrm{d}y\\
&\quad + \int_{x_0}^{x_0+\delta x} -h_t'(x)\tau(x,h_t(x)) + \sigma_y(x,h_t(x))\,\mathrm{d}x + \int_{x_0}^{x_0+\delta x} h_b'(x)\tau(x,h_b(x)) - \sigma_y(x,h_b(x))\,\mathrm{d}x.
\end{aligned}$$

Analogously, we have for the first two summands that

$$\begin{aligned}
&\int_{h_b(x_0+\delta x)}^{h_t(x_0+\delta x)} \tau(x_0+\delta x,y)\,\mathrm{d}y - \int_{h_b(x_0)}^{h_t(x_0)} \tau(x_0,y)\,\mathrm{d}y\\
&\quad = h_t'(x_0)\delta x \tau(x_0,h_t(x_0)) - h_b'(x_0)\delta x \tau(x_0,h_b(x_0)) + \delta x \frac{\partial}{\partial x}\int_{h_b(x_0)}^{h_t(x_0)} \tau(x_0,y)\,\mathrm{d}y\\
&\qquad - \delta x[\tau(x_0,h_t(x_0))h_t'(x_0) - \tau(x_0,h_b(x_0))h_b'(x_0)] + o(\delta x).
\end{aligned}$$

Therefore, dividing the force balance equation by δx and letting $\delta x \to 0$ we have in the limit

$$\begin{aligned}
0 &= h_t'(x_0)\tau(x_0, h_t(x_0)) - h_b'(x_0)\tau(x_0, h_b(x_0)) + \frac{\partial}{\partial x}\int_{h_b(x_0)}^{h_t(x_0)} \tau(x_0, y)\,\mathrm{d}y \\
&\quad - \tau(x_0, h_t(x_0))h_t'(x_0) + \tau(x_0, h_b(x_0))h_b'(x_0) \\
&\quad - h_t'(x_0)\tau(x_0, h_t(x_0)) + \sigma_y(x_0, h_t(x_0)) + h_b'(x_0)\tau(x_0, h_b(x_0)) - \sigma_y(x_0, h_b(x_0)) \\
&= \frac{\partial}{\partial x}\int_{h_b(x_0)}^{h_t(x_0)} \tau(x_0, y)\,\mathrm{d}y \\
&\quad - h_t'(x_0)\tau(x_0, h_t(x_0)) + \sigma_y(x_0, h_t(x_0)) + h_b'(x_0)\tau(x_0, h_b(x_0)) - \sigma_y(x_0, h_b(x_0))
\end{aligned}$$

or shorter

$$\partial_x \int_{h_b}^{h_t} \tau\,\mathrm{d}y = h_t'\tau(h_t) - h_b'\tau(h_b) + \sigma_y(h_b) - \sigma_y(h_t).$$

Integrating the moments counter clockwise around $(x_0, 0)$ along the boundary of the slab gives

$$\begin{aligned}
0 &= \int_{h_b(x_0)}^{h_t(x_0)} y\sigma_x(x_0, y)\,\mathrm{d}y + \int_{h_b(x_0+\delta x)}^{h_t(x_0+\delta x)} -y\sigma_x(x_0+\delta x, y) + \tau(x_0+\delta x, y)\delta x\,\mathrm{d}y \\
&\quad + \int_{x_0}^{x_0+\delta x} -h_b(x)\left[h_b'(x)\sigma_x(x, h_b(x)) - \tau(x, h_b(x))\right] \\
&\qquad + (x - x_0)\left[h_b'(x)\tau(x, h_b(x)) - \sigma_y(x, h_b(x))\right]\,\mathrm{d}x \\
&\quad + \int_{x_0}^{x_0+\delta x} h_t(x)\left[h_t'(x)\sigma_x(x, h_t(x)) - \tau(x, h_t(x))\right] \\
&\qquad + (x - x_0)\left[-h_t'(x)\tau(x, h_t(x)) - \sigma_y(x, h_t(x))\right]\,\mathrm{d}x.
\end{aligned}$$

The first two terms equal

$$\begin{aligned}
&\int_{h_b(x_0)}^{h_t(x_0)} y\sigma_x(x_0, y)\,\mathrm{d}y + \int_{h_b(x_0)+h_b'(x_0)\delta x}^{h_t(x_0)+h_t'(x_0)\delta x} -y\sigma_x(x_0, y) - y\frac{\partial \sigma_x}{\partial x}(x_0, y)\delta x + \tau(x_0, y)\delta x\,\mathrm{d}y + o(\delta x) \\
&= \left(\int_{h_t(x_0)}^{h_t(x_0)+h_t'(x_0)\delta x} - \int_{h_b(x_0)}^{h_b(x_0)+h_b'(x_0)\delta x}\right) - y\sigma_x(x_0, y)\,\mathrm{d}y \\
&\quad + \int_{h_b(x_0)}^{h_t(x_0)} -y\frac{\partial \sigma_x}{\partial x}(x_0, y)\delta x + \tau(x_0, y)\delta x\,\mathrm{d}y + o(\delta x) \\
&= -h_t'(x_0)\delta x h_t(x_0)\sigma_x(x_0, h_t(x_0)) + h_b'(x_0)\delta x h_b(x_0)\sigma_x(x_0, h_b(x_0)) \\
&\quad + \delta x\frac{\partial}{\partial x}\int_{h_b(x_0)}^{h_t(x_0)} -y\sigma_x(x_0, y)\,\mathrm{d}y \\
&\quad + \delta x\left[h_t'(x_0)h_t(x_0)\sigma_x(x_0, h_t(x_0) - h_b'(x_0)h_b(x_0)\sigma_x(x_0, h_b(x_0))\right] \\
&\quad + \delta x\int_{h_b(x_0)}^{h_t(x_0)} \tau(x_0, y)\,\mathrm{d}y + o(\delta x)
\end{aligned}$$

Therefore, dividing the moment balance equation by δx and letting $\delta x \to 0$ we have in the limit

$$\begin{aligned}
0 &= -h_t'(x_0)h_t(x_0)\sigma_x(x_0,h_t(x_0)) + h_b'(x_0)h_b(x_0)\sigma_x(x_0,h_b(x_0)) + \frac{\partial}{\partial x}\int_{h_b(x_0)}^{h_t(x_0)} -y\sigma_x(x_0,y)\,\mathrm{d}y \\
&\quad + h_t'(x_0)h_t(x_0)\sigma_x(x_0,h_t(x_0) - h_b'(x_0)h_b(x_0)\sigma_x(x_0,h_b(x_0)) + \int_{h_b(x_0)}^{h_t(x_0)} \tau(x_0,y)\,\mathrm{d}y \\
&\quad - h_b(x_0)\left[h_b'(x_0)\sigma_x(x_0,h_b(x_0)) - \tau(x_0,h_b(x_0))\right] + h_t(x_0)\left[h_t'(x_0)\sigma_x(x_0,h_t(x_0)) - \tau(x,h_t(x))\right] \\
&= \frac{\partial}{\partial x}\int_{h_b(x_0)}^{h_t(x_0)} -y\sigma_x(x_0,y)\,\mathrm{d}y + \int_{h_b(x_0)}^{h_t(x_0)} \tau(x_0,y)\,\mathrm{d}y \\
&\quad - h_b(x_0)\left[h_b'(x_0)\sigma_x(x_0,h_b(x_0)) - \tau(x_0,h_b(x_0))\right] + h_t(x_0)\left[h_t'(x_0)\sigma_x(x_0,h_t(x_0)) - \tau(x,h_t(x))\right]
\end{aligned}$$

or shorter,

$$\partial_x \int_{h_b}^{h_t} y\sigma_x\,\mathrm{d}y = \int_{h_b}^{h_t} \tau\,\mathrm{d}y + h_t\left[h_t'\sigma_x(h_t) - \tau(h_t)\right] - h_b\left[h_b'\sigma_x(h_b) - \tau(h_b)\right].$$

4.2.1 General Inner Model Equations

Let us summarise the equations that we have derived. For conventience, we shall write $\sigma_x(h_t) = \sigma_t$ and $\tau(h_t) = \tau_t$ (similar for $y = h_b$).

$$\partial_x \int_{h_b}^{h_t} \sigma_x\, y\, dy = \int_{h_b}^{h_t} \tau\, dy - h_t(-h_t'\sigma_t + \tau_t) - h_b(h_b'\sigma_b - \tau_b) \tag{EQ1}$$

$$\partial_x \int_{h_b}^{h_t} \tau\, dy = h_t'\tau_t - \sigma_y(h_t) - h_b'\tau_b + \sigma_y(h_b) \tag{EQ2}$$

$$\partial_x \int_{h_b}^{h_t} \sigma_x\, dy = h_t'\sigma_t - \tau_t - h_b'\sigma_b + \tau_b \tag{EQ3}$$

4.3 A Specific Inner Model

Equations (EQ1), (EQ2) and (EQ3) make no significant assumptions about the physics of the inner model, but they are underconstrained. In particular, we have differential equations in three averaged quantities and we need to also know the values of the stress tensor (σ_x, σ_y and τ) at both the top and bottom contact surfaces. Additional physical assumptions are needed in order to get a problem which is neither underconstrained nor overconstrained. The major assumptions that we shall use in this section are: a friction law at the top and bottom, where the workpiece contacts the roller; the workpiece is at yield at the top and bottom; the horizontal stress varies linearly through the thickness. This then leads to differential equations in σ_t, σ_b and $\overline{\tau}$ (the average shear stress). The friction law and yield condition allow us to write $\sigma_y(h_t)$ (resp. $\sigma_y(h_b)$) and τ_t (resp. τ_b) in terms of σ_t (resp. σ_b), thereby leaving us with three differential equations in three unknowns.

4.3.1 Assumptions: Friction Law, Yield Condition and Linear Stress

Define the modified sign functions,

$$\begin{aligned}\mathrm{sgn_t}(x) &= \mathrm{sgn}(x - x_t^n)\,\mathrm{hvsd}(x - x_t^{in})\,\mathrm{hvsd}(x_t^{out} - x),\\ \mathrm{sgn_b}(x) &= \mathrm{sgn}(x - x_b^n)\,\mathrm{hvsd}(x - x_b^{in})\,\mathrm{hvsd}(x_b^{out} - x),\end{aligned}$$

where hvsd is the Heaviside function: $hvsd(z) = 1$, $z \geq 0$ and 0 elsewhere. The friction law states that material is pushed towards the neutral point[1]. Mathematically, the friction law at the top and bottom of the rollers states:

$$\begin{aligned}\mu\left(h_t'^2\sigma_t - 2h_t'\tau_t + \sigma_y\right)\mathrm{sgn_t}(x) &= (1 - h_t'^2)\tau_t + (\sigma_y - \sigma_t)h_t'\\ -\mu\left(h_b'^2\sigma_b - 2h_b'\tau_b + \sigma_y\right)\mathrm{sgn_t}(x) &= (1 - h_b'^2)\tau_b + (\sigma_y - \sigma_b)h_b'.\end{aligned}$$

We assume that the deformation occuring at the roll surfaces is plastic, which means we have the yield condition:

$$\left(\frac{\sigma_x - \sigma_y}{2}\right)^2 + \tau^2 = k^2.$$

Our most controversial assumption is the linear variation of stress through thickness across the roll gap:

$$\sigma_x(y) = \frac{\sigma_t - \sigma_b}{\Delta h}y + \frac{\sigma_b h_t - \sigma_t h_b}{\Delta h}.$$

Evidence in support of this assumption is dubious. In his thesis [Min17], Minton had observed constant pressure across the roll gap in some flat rolling configurations. Other than this, there is little other reason to suppose this. Our main reason for this assumption is that it was the simplest assumption we could make in order to obtain a working example of an inner model given our time constraints.

4.3.2 Manipulating EQ1: An Equation For σ_b

Note that,

$$\partial_x \int_{h_b}^{h_t} \sigma_x y\,dy = h_t' h_t \sigma_t - h_b' h_b \sigma_b + \int_{h_b}^{h_t} \partial_x \sigma_x y\,dy,$$

which implies that (EQ1) becomes

$$\int_{h_b}^{h_t} \partial_x \sigma_x y\,dy = \Delta h\,\overline{\tau} - h_t\tau_t + h_b\tau_b.$$

Using the linear stress assumption and computing the derivative, we find:

$$\partial_x\sigma_x = \left(\frac{\partial_x\sigma_t - \partial_x\sigma_b}{\Delta h} - \frac{\sigma_t - \sigma_b}{(\Delta h)^2}\frac{d\Delta h}{dx}\right)y + \frac{h_t\partial_x\sigma_b + h_t'\sigma_b - h_b\partial_x\sigma_t - h_b'\sigma_t}{\Delta h} - \frac{\sigma_b h_t - \sigma_t h_b}{(\Delta h)^2}\frac{d\Delta h}{dx}.$$

[1] We assume the existence of one neutral point per roller.

Hence,

$$\begin{aligned}\int_{h_b}^{h_t}\partial_x\sigma_x y\,dy &= \left(\frac{\partial_x\sigma_t-\partial_x\sigma_b}{\Delta h}-\frac{\sigma_t-\sigma_b}{(\Delta h)^2}\frac{d\Delta h}{dx}\right)\frac{(h_t^3-h_b^3)}{3}+\\ &+\left(\frac{\partial_x\sigma_b h_t-\partial_x\sigma_t h_b}{\Delta h}+\frac{\sigma_b h_t'-\sigma_t h_b'}{\Delta h}-\frac{\sigma_b h_t-\sigma_t h_b}{(\Delta h)^2}\frac{d\Delta h}{dx}\right)\frac{(h_t^2-h_b^2)}{2}\\ &=\left(\frac{h_t^3-h_b^3}{3\Delta h}-\frac{h_b(h_t^2-h_b^2)}{2\Delta h}\right)\partial_x\sigma_t+\left(-\frac{h_t^3-h_b^3}{3\Delta h}+\frac{h_t(h_t^2-h_b^2)}{2\Delta h}\right)\partial_x\sigma_b+\\ &+\left(-\frac{(\sigma_t-\sigma_b)(h_t^3-h_b^3)}{3(\Delta h)^2}-\frac{(\sigma_b h_t-\sigma_t h_b)(h_t^2-h_b^2)}{2(\Delta h)^2}\right)\frac{d\Delta h}{dx}+\frac{(\sigma_b h_t'-\sigma_t h_b')(h_t^2-h_b^2)}{2\Delta h}\\ &=\left(\frac{2h_t^2-h_bh_t-h_b^2}{6}\right)\partial_x\sigma_t+\left(\frac{-2h_b^2+h_bh_t+h_t^2}{6}\right)\partial_x\sigma_b+\\ &+\left(\frac{-2h_t^2+h_th_b+h_b^2}{6\Delta h}\sigma_t+\frac{2h_b^2-h_th_b-h_t^2}{6\Delta h}\sigma_b\right)\frac{d\Delta h}{dx}+\frac{(\sigma_b h_t'-\sigma_t h_b')(h_t+h_b)}{2}.\end{aligned}$$

Putting this back into our differential equation and rearranging, we find a differential equation for σ_b:

$$\begin{aligned}\partial_x\sigma_b &= \frac{6}{-2h_b^2+h_th_b+h_t^2}\left(\Delta h\,\overline{\tau}-h_t\tau_t+h_b\tau_t\right)+\left(-\left(\frac{-2h_t^2+h_th_b+h_b^2}{-2h_b^2+h_th_b+h_t^2}\right)\sigma_t+\sigma_b\right)\frac{1}{\Delta h}\frac{d\Delta h}{dx}-\\ &-\frac{3(\sigma_b h_t'-\sigma_t h_b')(h_t+h_b)}{-2h_b^2+h_th_b+h_t^2}+\left(\frac{-2h_t^2+h_th_b+h_b^2}{-2h_b^2+h_th_b+h_t^2}\right)\partial_x\sigma_t.\end{aligned}$$

The form of the above equations suggests to introduce geometric quantities,

$$\begin{aligned}\rho_t &= -2h_t^2+h_th_b+h_b^2,\\ \rho_b &= -2h_b^2+h_th_b+h_t^2.\end{aligned}$$

The quantity $\frac{\rho_t}{\rho_b}$ measures the asymmetry of the roll geometry - indeed, it is 1 for symmetric rolls of the same radius. In order to see this better, note that

$$\frac{\rho_t}{\rho_b}=\frac{2h_t+h_b}{2h_b+h_t}=\frac{2\frac{h_t}{h_b}+1}{2+\frac{h_t}{h_b}}.$$

Our equation then becomes,

$$\partial_x\sigma_b=\frac{6}{\rho_b}\left(\Delta h\,\overline{\tau}-h_t\tau_t+h_b\tau_b\right)+\left(-\frac{\rho_t}{\rho_b}\,\sigma_t+\sigma_b\right)\frac{1}{\Delta h}\frac{d\Delta h}{dx}-\frac{3(\sigma_b h_t'-\sigma_t h_b')(h_t+h_b)}{\rho_b}+\frac{\rho_t}{\rho_b}\,\partial_x\sigma_t.$$

4.3.3 Manipulating EQ2: An Equation For $\overline{\tau}$

We have the equation,

$$\partial_x\int_{h_b}^{h_t}\tau\,dy=h_t'\tau_t-\sigma_y(h_t)-h_b'\tau_b+\sigma_y(h_b).$$

Notincg that,

$$\int_{h_b}^{h_t}\tau\,dy=\Delta h\,\overline{\tau},$$

it is a straightforward computation to show that

$$\partial_x \overline{\tau} = \frac{1}{\Delta h}\left(h_t'\tau_t - \sigma_y(h_t) - h_b'\tau_b + \sigma_y(h_b) - \overline{\tau}\frac{d\Delta h}{dx}\right).$$

4.3.4 Manipulating EQ3: An Equation For σ_t

Using the fundamental theorem of calculus on the first term in the differential equation

$$\partial_x \int_{h_b}^{h_t} \sigma_x \, dy = h_t'\sigma_t - \tau_t - h_b'\sigma_b + \tau_b,$$

yields the new equation

$$\int_{h_b}^{h_t} \partial_x \sigma_x \, dy = -\tau_t + \tau_b.$$

Let us calculate this integral using the linearity assumption.

$$\begin{aligned}
\int_{h_b}^{h_t} \partial_x \sigma_x dy =& \int_{h_b}^{h_t} \left(\frac{\partial_x\sigma_t - \partial_x\sigma_b}{\Delta h} - \frac{\sigma_t - \sigma_b}{(\Delta h)^2}\frac{d\Delta h}{dx}\right) y \, dy \\
&+ \int_{h_b}^{h_t} \left(\frac{h_t\partial_x\sigma_b + h_t'\sigma_b - h_b\partial_x\sigma_t - h_b'\sigma_t}{\Delta h} - \frac{\sigma_b h_t - \sigma_t h_b}{(\Delta h)^2}\frac{d\Delta h}{dx}\right) dy \\
=& \frac{(\partial_x\sigma_t - \partial_x\sigma_b)(h_t + h_b)}{2} - \frac{\sigma_t - \sigma_b}{2}\frac{h_t + h_b}{\Delta h}\frac{d\Delta h}{dx} \\
&+ (h_t\partial_x\sigma_b + h_t'\sigma_b - h_b\partial_x\sigma_t - h_b'\sigma_t) - \frac{\sigma_b h_t - \sigma_t h_b}{\Delta h}\frac{d\Delta h}{dx} \\
=& (\partial_x\sigma_t + \partial_x\sigma_b)\frac{\Delta h}{2} - \frac{\sigma_t + \sigma_b}{2}\frac{d\Delta h}{dx} + h_t'\sigma_b - h_b'\sigma_t.
\end{aligned}$$

Using the above, we obtain the differential equation

$$\partial_x\sigma_t = \frac{2}{\Delta h}(-\tau_t + \tau_b - h_t'\sigma_b + h_b'\sigma_t) + \frac{\sigma_t + \sigma_b}{\Delta h}\frac{d\Delta h}{dx} - \partial_x\sigma_b.$$

In Appendix A, we continue analysing this specific inner model by using friction laws and the yield condition to eliminate unknowns, so that we can implement our set of differential equations numerically.

5 Numerical Results

5.1 Implementation

We implement the inner model and a simplified version of the outer model as a combined package in MATLAB[2]. Our results are displayed in Figures 6, 7, 8, 9, 10, 11, 12 and 13 found in Appendix B. In each figure: the first plot is of the horizontal stresses at the top and bottom, as well as the average shear stress, against the displacement across the roll gap; the second plot is of the horizontal

[2]Our package has been uploaded to https://warwick.ac.uk/fac/sci/masdoc/current/msc-modules/ma916/mnr/.

and vertical forces, and moment abouts about the zero-line[3] as the displacement across the roll gap varies. In both of these plots, vertical lines correspond to contact or neutral points, with darker lines indicating the top roll[4]. The third plot, in figures with curved ring geometries, is of the predicted ring profile for an undeformed circular ring of radius 3m subjected to the forces and moments obtained at the end of the inner model regime.

The code for the inner model presents a complete, flexible numerical model modulo the assumptions that: the horizontal stress varies linearly through the thickness; the beam is at yield when in contact with the rollers; and that we have a friction law at the roll surfaces. As inputs, it takes roll geometry, contact and neutral points for the metal ring, initial horizontal stress at the top and bottom, and initial average shear stress. In turn, the code returns: the horizontal stresses at the top, at the bottom, and the average shear stress, throughout the roll gap; the horizontal and vertical forces, as well as the moment, across the roll gap. These are then plotted against the displacement across the roll gap. The model, on its own, does not require specification of: the initial width or curvature of the beam; the aspect ratio and reduction whether elastic recovery or perfect plasticity occurs; the roll speeds, curvature prediction to predict exit points and exit curvatures. Indeed, specification of the aforementioned quantities could allow one to locate the four contact points and one of the two neutral points. The numerical solutions of the inner model should be interpreted as being valid for physical rolling problems which yield those contact and neutral points.

The code for the outer model is a simplified code that can only support circular rings. The reason why we have a simplified code is that we wanted to test what deformations would occur to an undeformed, circular beam subject to the forces obtained at the end of the inner model. Curvature and circularity changes were our key points of focus. In order to incorporate more general rings, an explicit parametrisation of the initial ring is needed and the code can be adapted accordingly. The key inputs of the model, as it stands, are: the radius of the undeformed ring; the thickness of the ring; angular displacements that mark the start and end points of the outer model; and, finally, the forces and moments at one end of the beam. The output is a plot of the deformed ring profile.

In order to use the outer model code to test deformation predictions under forces generated by the inner model, a toy coupling[5] is needed. Throughout all simulations of the inner model, we keep the length of roll gap roughly around 40mm. Since we keep the radius of the ring fixed at 3m, this suggests an angular displacement of 0.134 radians is needed between the ends of the outer model. Moreover, we make a simplifying assumption that the width of the beam is taken to be the width of closest separation of the rolls. This is of course false in general but for ring rolling configurations with small reduction and large ring radius (with respect to the roll gap length), this approximation seems sensible. Our final assumption is that the forces and moments at the ends of the beam in the outer model are taken to be the forces and moments predicted by the inner model at the point $\frac{x_t^{out}+x_b^{out}}{2}$.

In order to test the physical validity of our model predictions, we aimed to include some numerical checks against governing equations. For the inner model, such a check seems out of reach without more knowledge about the physics away from the rollers. This manifests in the fact that our equations do not give the whole stress tensor in the roll gap; rather, it gives the horizontal stress and the average shear stress. For the outer model, the physics suggests that the work done in displacing the beam should be equal to the strain energy. The function *workError* encodifies this check, and is

[3]Recall that $y = h_t(x)$ and $y = h_b(x)$ are global parametrisations of the rollers. The zero-line is just the line $y = 0$.

[4]When these points coincide, MATLAB favours the lighter grey line, which indicates the bottom roll.

[5]We call this a toy coupling because it is not a coupling of the inner and outer models to give a ring rolling model. Rather, it should be interpreted as seeing the effect of forces produced in the inner model on the outer model.

used in *pproc.m*.

5.2 Analysis of Results

5.2.1 Flat Sheet Rolling

Figures 6 and 7 display numerical results for flat sheet - both thick and thin - rolling configurations in our inner model[6]. Here, thin and thick refer to the aspect ratio which, since we keep the length of the roll gap of the same order, is changed by changing the minimum separation of the rolls. Thin refers to a separation of 0.05m, whereas thick refers to a separation of 1m. The purpose of these figures is to provide a way to check the reliability and accuracy of the model in the simplified case of no curvature of the incident beam and no asymmetry of the rolls. Indeed, by cross-referencing with existing models of thin-sheet rolling, we can try to ascertain whether key behaviours of thin-sheet rolling are captured by our model. We assume that the neutral points of the top and bottom rolls coincide. This is a reasonable assumption since models of symmetric, thin-sheet rolling predict coincidence of neutral points. Our key assumption, however, is linear variation of the horizontal stress through thickness (y-direction) of the workpiece. A rigorous numerical analysis is yet to be carried out to validate the model, and its assumptions, in these regimes. In general, one does not expect that the assumption of linear variation of the horizontal stress to always hold. Nevertheless, we highlight key qualitative features in common and in contrast to existing models.

Analytical models of symmetric, flat thin-sheet rolling exist in the literature - see Chapters 1 and 2 of [Min17] - and two important characteristics of symmetric, thin-sheet rolling that one obtains from these models are the existence of a pressure hill and discontinuity and in shear stress across the neutral point. Here, pressure hill means that the pressure is largest in size at the neutral point and decreases to near zero at the entry and exit points of the rollers. The plot of the horizontal stresses implicitly incorporates the pressure since the horizontal stress is the deviatoric horizontal stress minus the pressure. Assuming that the deviatoric stress is much smaller than the pressure term, the first plot of Figure 6 suggests such a pressure hill occurs. The discontinuity in shear stress cannot be seen in our models since we use the average shear stress, but the symmetry of the shear stress at the top and bottom can. This is precisely why the average shear stress is 0. These observations are encouraging for our model of ring rolling and, if further tests continue to highlight agreement with existing observations of thin-sheet rolling, validate the assumption of linear variation of horizontal stress.

For thick-sheet rolling, an analytical model was proposed in [Min17], Chapter 5, but remains incomplete. The key feature of this model is the occurence of shear stress oscillations. Due to the lack of dependence of our model on aspect ratio, the inner model results in Figure 7 are a scaling of that of thin-sheet rolling. Hence, any non-linear behaviour that is unique to the physics of thick-sheet rolling is not captured by our model. In particular, shear stress oscillations are not captured. Furthermore, it is not clear whether the assumption of linear variation of horizontal stress is valid. It would be interesting to see whether the additional physics involved in thick-sheet rolling can be incorporated into our model and to see whether results captured in [Min17], Chapter 5 can be replicated and extended. To summarise, further investigation is required in this case.

[6]There is also plots of deformations to an artificial outer model. This was added more of a curiosity rather than anything; those plots are more important for curved geometries. One could, however, argue that in a large ring limit, the inner model would be flat sheet rolling.

5.3 Curved Beam Rolling

Figures 8 and 9 display results for a curved beam with moderate aspect ratio undergoing symmetric and asymmetric, respectively, rolling. We chose a moderate aspect ratio, manifested in the minimum roll separation being 0.3m, with the hope that the linear variation of stress could be approximately true. There is no evidence, however, for curved beams that linear variation of horizontal stress through thickness could be valid for small aspect ratios. Rigorous numerical tests and finite element simulations are yet to be carried out. Nevertheless, we highlight key qualitative features of the model.

The stress plots in Figure 8 shows horizontal stresses at the bottom and average shear stresses of the order of 10^6 to 10^7 Pa near the exit region, whilst horizontal stresses at the top are clearly of order of 10^7 Pa near the exit region. The effect of the contact and neutral points on the rolling model can clearly be seen as discontinuities in the gradient of these stresses. As expected, despite the symmetry of the roll configuration, likely due to the curved nature of the problem, the horizontal stresses at the top and bottom are not symmetric. Moreover, we do not have symmetry in the shear stress since the average shear stress is oscillating about 0. Unlike the former property, this is potentially interesting non-linear behaviour and will be discussed in the next subsection. We did assume that the neutral points coincide, which may not be a realistic phenomenon of curved rolling even with symmetric rolls; however, it could be possible to make the neutral points coincide by adjusting the ratio of the roll speeds. The second plot shows forces and moments. The effect of contact and neutral points on force production are clearly shown for the forces; for the moment, interesting oscillatory behaviour is shown. The forces at the end of the roll gap are of order 10^6 N and the moments are of order 10^6 Nm. As evidenced in the third plot, these cause severe deformation of the ring, twisting the ends across each other. This implies that the dataset used may be inappropriate for a model of ring rolling: either the geometries are incompatible or the forces produced by the inner model are too large to be coupled to an elastic beam.

The stress plots in Figure 9 also clearly show horizontal stresses at the bottom and at the top, and average shear stresses of the order of 10^8 Pascals near the exit region. The second plot indicates that forces and moments are of the order 10^7 Newtons and Newtonmetres. The effects of the contact and neutral points on the horizontal stresses and both forces are again as discontinuities in the gradient. Interesting oscillatory phenomena with the average shear stress and moment is also present, with similar period. The effects of these large forces and moments is considerable, though not severe, deformation of the ring, as seen in the third plot. This could suggest that larger aspect ratios may be more suitable for ring rolling models.

These figures show off the potential use of our inner model of analysing curved beams. After subjecting the model to rigorous numerical testing, it would be fascinating to explore phenomena such as curvature production or oscillations of shear stresses in curved, asymmetric rolling prolems. Indeed, the potential occurence of oscillations of shear stresses in curved beams with moderate aspect ratios is surprising and could be an indicator that such behaviour may be intrinsic to the physics of rolling. With regards to the deformations of the outer model, the fact that they are significant could indicate that the rolling configurations presented - in particular, neutral points, contact points and minimum separation of the rolls - are not suitable for ring rolling problems. This is speculative, and a numerical investigation into this is the obvious next step.

5.4 Dependency On Aspect Ratio

Putting aside issues of numerical validity, we try to use our inner model to investigate the dependency of curved, asymmetric rolling problems on the aspect ratio. The precise rolling configurations are indicated in Figures 10, 11, 12 and 13. We keep all features of the rolling problem the same except for the minimum separation of the rolls which, as we have argued before, is essentially varying the aspect ratio.

In terms of the effect on the deformations in the outer model, one can clearly see from the third plots in the above figures that larger aspect ratios lead to milder deformations. Indeed, for the rings of thickness 0.5m and 1m, it seems as though coupling could be plausible if some parameters are fine tuned. We note that the milder deformations is not entirely due to the magnitudes of the forces and moments being lessened - they are all, in fact, roughly of order 10^7 as we vary the aspect ratio; rather, it seems as though greater symmetry of the forces near the end region of the roll gap is present for larger aspect ratios. This may be an error from the linear stress assumption, or a genuine artefact of the inner model.

The truly interesting feature in our comparison is oscillatory behaviour of not only the average shear stress, but also the horizontal and vertical shear stresses near the top and bottom of the rollers at small aspect ratios. These oscillations seem to dampen out as the aspect ratio increases, leading to a greater symmetry of the end region forces and moments, which in turns leads to stabilisation of the ring deformations. Of course, there is the potential issue with linear variation of horizontal stress being invalid for large aspect ratios (or, indeed, small aspect ratios of curved geometries). Indeed, in flat sheet rolling oscillations of shear stresses are observed in Minton's thick-sheet model but these results do not seem to corroborate this behaviour for thick-ring rolling. Moreover, there is a possibility that such oscillations are a manifestation of a numerical error. On the other hand, there is the possibility that such behaviour is intrinsic to the physics of nonlinear rolling problems. Clearly, then, there is a case for further investigation to be carried out.

6 Coupling

Coupling the inner and outer models is the most important step in obtaining a static ring rolling model. The statics problem can be understood in the following way. Take a curved beam undergoing elastic deformation, with some displacement between the ends, this is the outer model. The displacement between the endpoints corresponds to the roll gap: this is the inner model. Strictly speaking, one of the endpoints of the outer model corresponds to the midpoint, on the centreline, of the entry points of the workpiece into the roll gap; the other endpoint corresponds to the midpoint, on the centreline, of the exit points of the workpiece out of the roll gap. We assume that the forces at the end points of the outer model are much smaller in magnitude than the forces involved in the inner model, so we take zero entry horizontal and average shear stress conditions for the inner model. The inner model then gives us the forces and displacements at the end of the roll gap. At this stage, the system - that is, the inner and outer model combined - is possibly out of equilibrium. By out of equilibrium we mean that the models are incompatible, for example the outer model may predict the ring does not return to the roll gap. Coupling is achieved if the system is in equilibrium.

In order to understand what equilibrium really means, we need to understand what we have control over. We want to find a ring geometry for the outer model: that is, centreline parametrisation, thickness profile and angular displacements between the ends. Given these things, and the forces acting on the end of the beam, the outer model predicts the displaced beam, this displaced beam

must match the geometry of the inner model, so this information also fix the position of the contact points on the rolls. We are free to vary the neutral points of the inner model. If we fix the ratio of the roll speeds then we are able to determine one of the neutral points given the other[7]. Assuming linear variation of horizontal stress we can calculate the average shear stress and horizontal stresses at the top and bottom of the roller at the start of the inner model.[8] Solving the ODEs allows us to calculate the average shear stress and horizontal stresses at the top and bottom of the roller at the end of the inner model. We can then find forces and moments at this point but, since the outer ring is in equilibrium, we require that these forces and moments match the entry forces. Thus, we have control over the ring geometry and one of the neutral points, and we have a constraint on the end point forces and moments.

Mathematically, this can be rephrased as an optimisation/root-finding problem. The idea is to rewrite the inner and outer models as functions, taking all sufficient inputs and returning data necessary to achieve coupling. Let us make this precise. Suppose that variables $(v_1, \dots, v_j)$ are sufficient inputs for the inner model and $(v_{j+1}, \dots, v_n)$ are sufficient inputs for the outer model, where each variable v_i is an element of the normed vector space V_i. Furthermore, suppose that variables $(w_1, \dots, w_m)$ are the necessary outputs required to match the two models, where w_i is an element of the normed vector space W_i. In other words, we suppose that there exists functions g_{inner} and g_{outer} on V such that

$$g_{inner}(v) = w_i \in W_i, \quad g_{outer}(v) = \tilde{w}_i \in W_i, \tag{4}$$

and that for coupling we require $g_{inner}(v) = g_{outer}(v)$ or, equivalently, $w_i = \tilde{w}_i$. Then we can write the inner and outer models as functions,

$$F_{inner} \colon V \to W, \quad F_{outer} \colon V \to W, \tag{5}$$

where $V = \prod_{i=1}^{n} V_i$ and $W = \prod_{i=1}^{m} W_i$.

A full coupling of the two models is then the (fully) hard constraint problem: for $K \subset V$, find $v \in K$ such that

$$F_{inner}(v) = F_{outer}(v). \tag{6}$$

Solutions to this may be hard to find, especially if V is high-dimensional, so partial coupling could be achieved by considering the (fully) soft constraint problem: for $K \subset V$, find $v \in K$ that minimises the quantity

$$\|F_{inner}(v) - F_{outer}(v)\|_V. \tag{7}$$

Solutions to this may be easier to obtain but may not represent physical rolling configurations. This is a consequence that the minimiser may not make the above quantity be 0. Adding some hard constraints into the mix leads to a mixed soft-hard constraint problem. The adding of hard constraints will make finding a minimum harder so these should be added one at a time until a physically plausible solution is obtained. Existence of multiple solutions may suggest that the problem is underconstrained - meaning that we have not identified all necessary outputs; existence of no solutions may suggest that the problem is overconstrained - meaning that we have identified too many outputs.

[7] This assumes the existence of two neutral points.

[8] This is the first time when this assumption is used. For more general inner models, arguments might have to be adapted.

We were not able to implement the coupling numerically - perhaps it could be done using, for example, a black box solver such as *fmincon* in MATLAB - but we did lay some groundwork for future work to be done. For the rest of this section, we will make the input space V explicit and try to identify what we thought were the necessary outputs to achieve coupling.

6.1 Identifying the Input and Output spaces

The inputs for the inner model are the four contact points, two neutral points, the entry horizontal stresses at the top and bottom of the roller, and the entry average shear stress. Note that we also need to know the yield stress, the coefficient of friction of the rolls, the minimum separation of the rolls and the radii of the rolls. We do not seek to optimise these values; they are kept constant in the rolling problem. Hence, we do not include them in the input space. Moreover, knowing the ratio of the roll speeds allows us to determine one neutral point from the other, reducing the input variables by 1. This leads the input space for the inner model being $\mathbb{R}^8$.

The inputs for the outer model are the two end point angular displacements, the parametrisation of the centreline, the thickness profile of the ring and the forces and moment at one end of the beam. Held fixed in the outer model are the the cross-sectional profile of the ring, Young's modulus and the shear modulus. The outer model can then calculate the displacements between the ends under these forces. These displacements, together with the thickness profile can then be used to calculate the contact points. Our input space for the outer model is therefore $\mathbb{R}^3 \times \mathbb{T} \times \mathbb{T} \times C^2(\mathbb{T}) \times C^0(\mathbb{T})$. Here $\mathbb{T}$ refers to the torus on $[0, 2\pi]$, $C^2(\mathbb{T})$ is the space of twice continuously differentiable functions on the torus[9], $C^0(\mathbb{T})$ is the space of continuous functions on the torus. These correspond with the three forces, the two angles giving where the beam hits the roll gap, the parametrisation of the beam and the corresponding thickness profile, respectively.

We noted before that specifying the ring geometry and forces gives us the contact points for the inner model, meaning that 4 real variables in the inner model input space are not needed in the combined input space. Moreover from these forces we can deduce the horizontal stresses at the top and bottom, and the average shear stress from this, so we take them as inputs instead. This consideration means that the total input space for both problems is $\mathbb{R}^3 \times \mathbb{R} \times \mathbb{T} \times \mathbb{T} \times C^2(\mathbb{T}) \times C^0(\mathbb{T})$, corresponding to the three forces, the neutral point, the two angular displacements of the end points, the centreline parametrisation and the width profile.

Identifying the necessary outputs that need to be matched in order to achieve coupling is by no means a simple task and we do not claim to have fully solved this. First, let us treat forces and moments. On the one hand, by assumption of force balance on the beam, the forces and moment at the ends of the beam must balance. On the other hand, since we know the forces and moment on entry, we can calculate the horizontal stresses and the average shear stress at the point of entry[10]. By solving the ODEs and integrating the stresses we can find the forces and moment on the other

[9] We need at least two derivatives for the parametrisation of the centreline so that curvatures could be calculated

[10] Note that there is a slight error here because we take the start point of the outer model as the midpoint of the entry points of the inner model. This can be circumvented by taking 0 entry conditions on the horizontal stresses and average shear stress, which uses the assumption that elastic forces in the outer model are much smaller than the forces in the inner model. With this modelling assumption, however, it seems unreasonable to impose the agreement of entry and exit forces as a hard constraint; rather, a soft constraint should be used.

end. Coupling says that these should be equal, modulo hard or soft constraint:

$$F_{hoz} = \Delta h(A)\frac{\sigma_t(A) + \sigma_b(A)}{2} = \Delta h(B)\frac{\sigma_t(B) + \sigma_b(B)}{2}, \tag{8}$$

$$F_{ver} = \Delta h(A)\overline{\tau}(A) = \Delta h(B)\overline{\tau}(B), \tag{9}$$

$$M = \Delta h(A)\frac{-\sigma_t(A) + \sigma_b(A)}{2} = \Delta h(B)\frac{-\sigma_t(B) + \sigma_b(B)}{2}. \tag{10}$$

Given the ring geometry and given a neutral point. Combining this with the geometric constraint on the outer model we get the output space $W = \mathbb{R}^3 \times \mathbb{R}^4$, corresponding to the forces and the 4 contact points.

The lack of other constraints may be a manifestation of the fact that asking to optimise over ring geometries is too broad. Indeed, this involves optimisation over infinite dimensional vector spaces and it may not be straightforward to implement numerically. This suggests further assumptions should be made on the shape of the outer ring to get a practical numerical scheme. The hope would be to turn it into an optimisation problem over a finite dimensional vector space. Minton suggests REFERENCE that matching input and output curvatures could be used as a further constraint but we were not able to further pursue this.

6.2 A Possible Alternative

Coupling of the inner and outer model arises from the fact that we treat the physics governing the two models as fundamentally different: the inner model is governed by plastic deformation and the outer model is governed by elastic deformation. This may not be the case. The general equations for the inner model that we derived made no assumption about the physics of the roll gap. Indeed, instead of assuming the contact surface with the rollers were at yield, we could use the equations of elasticity throughout. It would be interesting to investigate whether Timoshenko's beam theory is obtained in this limit. This would mean that the outer model and inner model are governed by the same equations but with different boundary conditions. This would circumvent the problem of coupling but would involve more complicated boundary conditions; however, it may be the case that there are more tools available to deal with this case. Indeed, adding extra layers to the model - for example, a transition layer between the elastic and plastic regions - could be implemented by changing boundary conditions as opposed to achieving a simultaneous coupling of three models. Continuing in this vein, such an approach would also be more viable to model a series of rollers.

7 Concluding Remarks

The main contributions of this report are: a very general inner model, with consistent sign convention and no assumption on the physics except basic laws of continuum mechanics; the beginnings of a numerical investigation of the inner model, and produced force effects on the otuer model, on the assumptions of plastic deformation at the roll surfaces, friction laws and linear variation of horizontal stress through thickness in the roll gap; and, although we did not achieve coupling, we outlined the beginnings of a mathematical approach to coupling the two models as well as a possible alternative.

The equations (EQ1), (EQ2) and (EQ3) presented in Section 4 follow from force and moment balances on slabs (infinitesimal wedges in the roll gap). There are no other assumptions on the physics of the roll gap, and neither are there any major assumptions on the geometry (other than

explicit, global parametrisations of the rollers). We derive differential equations for three averaged quantities,

$$\int_{h_b}^{h_t} \sigma_x \, dx, \quad \int_{h_b}^{h_t} \tau \, dy, \quad \int_{h_b}^{h_t} \sigma_x y \, dy \tag{11}$$

and we need to know the behaviour of $\sigma_x(h_t), \sigma_x(h_b), \sigma_y(h_t), \sigma_y(h_b), \tau(h_t), \tau(h_b)$. The point is that they can be adapted to different physical rolling systems so long as the above quantities are specified, and it would be fascinating to see whether it is possible to adapt our model to thick-sheet rolling, elastic rolling and clad-sheet rolling.

Although our equations are general, the system is underconstrained: in order to provide the right amount of constraints, we assumed linear variation of stress through the thickness, friction laws and that the material was at yield on contact with the roll surface. Our main failing was that we were not able to justify the linear variation of stress assumption: indeed, it is not likely that this is true for large aspect ratios. We were, however, able to successfully run numerical simulations of the inner model. The beginnings of an investigation into dependence of the force production at the end of the roll gap on the aspect ratio was presented, along with our surprising findings of shear stress and horizontal stress oscillations for small aspect ratios. A rigorous numerical investigation into our model is the next obvious step in this vein. We would find it very interesting to numerically investigate whether the stress oscillations are a numerical error or an intrinsic part to nonlinear rolling problems.

Our work towards coupling the model was less successful. The main failing of this investigation into ring rolling was the failure to achieve a coupling of the two models. This being said, we rephrased the coupling problem in terms of a constrained optimisation problem. We identified the inputs for both the inner and outer models, and suggested some contraints. Future work would naturally be to continue working on identifying the correct constraints.

We briefly described a possible alternative approach[11] to ring rolling that circumvents the issue of coupling. The idea is to see whether the general inner model that we have would yield Timoshenko's beam theory if this inner model was coupled with the laws of elasticity theory. If correct, then this would be an intriguing point of departure to consider ring rolling as governed by the same equations - that is, our general inner model equations - but with complicated boundary conditions. One could argue that this is swapping one difficult issue (the coupling) for another (the boundary condition), but we feel that, due to the sensitivity of both models to changes in input data, the boundary condition issue could be easier to deal with. We end this report, then, with the hope that this idea is explored further at some point in the future.

[11] This was suggested to us by one of our supervisors, Ed Brambley.

Appendices

A Inner Model Derivations

A.0.1 An Alternate Equation For σ_b

For the numerics, we require to eliminate the dependence of $\partial_x\sigma_b$ on $\partial_x\sigma_t$. This can be achieved by substituting the differential equation that we had obtained for $\partial_x\sigma_t$. Explicitly:

$$\left(1+\frac{\rho_t}{\rho_b}\right)\partial_x\sigma_b = \frac{6}{\rho_b}(\Delta h\,\overline{\tau} - h_t\tau_t + h_b\tau_b) + \left(-\frac{\rho_t}{\rho_b}\sigma_t + \sigma_b\right)\frac{1}{\Delta h}\frac{d\Delta h}{dx} - \\ - \frac{3}{\rho_b}\left(\sigma_b h_t' - \sigma_t h_b'\right)(h_t + h_b) + \frac{\rho_t}{\rho_b}\frac{2}{\Delta h}(-\tau_t + \tau_b - h_t'\sigma_b + h_b'\sigma_t) + \frac{\rho_t}{\rho_b}\frac{\sigma_t+\sigma_b}{\Delta h}\frac{d\Delta h}{dx}.$$

By rewriting $1+\frac{\rho_t}{\rho_b}$ as $\frac{\rho_b+\rho_t}{\rho_b}$, we get a nice form for $\partial_x\sigma_b$:

$$\partial_x\sigma_b = \frac{6}{\rho_b+\rho_t}(\Delta h\,\overline{\tau} - h_t\tau_t + h_b\tau_b) + \frac{\rho_b}{\rho_b+\rho_t}\left(-\frac{\rho_t}{\rho_b}\sigma_t + \sigma_b\right)\frac{1}{\Delta h}\frac{d\Delta h}{dx} - \\ - \frac{3}{\rho_b+\rho_t}\left(\sigma_b h_t' - \sigma_t h_b'\right)(h_t + h_b) + \frac{\rho_t}{\rho_b+\rho_t}\frac{2}{\Delta h}(-\tau_t + \tau_b - h_t'\sigma_b + h_b'\sigma_t) + \frac{\rho_t}{\rho_b+\rho_t}\frac{\sigma_t+\sigma_b}{\Delta h}\frac{d\Delta h}{dx}.$$

A.0.2 Eliminating Unknowns

The unknowns are $\tau_t, \tau_b, \sigma(h_t)$ and $\sigma(h_b)$. To eliminate them, we use the friction law and yield conditions at the top and at the bottom.

First, let us use the friction laws to obtain expressions for τ_t and τ_b in terms of σ_t and σ_y:

$$\tau_t = \frac{\mu\left(h_t'^2\sigma_t + \sigma_y\right)\mathrm{sgn_t} - (\sigma_y - \sigma_t)h_t'}{1 - h_t'^2 + 2\mu h_t'\mathrm{sgn_t}},$$
$$\tau_b = \frac{-\mu\left(h_b'^2\sigma_b + \sigma_y\right)\mathrm{sgn_b} - (\sigma_y - \sigma_b)h_b'}{1 - h_b'^2 - 2\mu h_b'\mathrm{sgn_b}}.$$

Splitting this up into coefficients for σ_y and σ_t, we can rewrite the above as

$$\tau_t = C_t\sigma_y + D_t\sigma_t, \quad \tau_b = C_b\sigma_y + D_b\sigma_b,$$

where

$$C_t = \frac{\mu\mathrm{sgn_t} - h_t'}{1 - h_t'^2 + 2\mu h_t'\mathrm{sgn_t}},$$
$$C_b = \frac{-\mu\mathrm{sgn_b} - h_b'}{1 - h_b'^2 - 2\mu h_b'\mathrm{sgn_b}},$$
$$D_t = \frac{\mu h_t'^2\mathrm{sgn_t} + h_t'}{1 - h_t'^2 + 2\mu h_t'\mathrm{sgn_t}},$$
$$D_b = \frac{-\mu h_b'^2\mathrm{sgn_b} + h_b'}{1 - h_b'^2 - 2\mu h_b'\mathrm{sgn_b}}.$$

Putting this into the yield equation and rearranging, we obtain:

$$\left(\frac{1}{4}+C_t^2\right)\sigma_y^2+\left(2C_tD_t-\frac{1}{2}\right)\sigma_t\sigma_y+\left(\frac{1}{4}+D_t^2\right)\sigma_t^2-k^2=0,$$
$$\left(\frac{1}{4}+C_b^2\right)\sigma_y^2+\left(2C_bD_b-\frac{1}{2}\right)\sigma_b\sigma_y+\left(\frac{1}{4}+D_b^2\right)\sigma_b^2-k^2=0.$$

We make the ansatz that $\sigma_y \gg \sigma_x$, so that we take the largest root of the quadratic:

$$\sigma_y(h_t)=\frac{-\left(2C_tD_t-\frac{1}{2}\right)\sigma_t+\sqrt{\left(2C_tD_t-\frac{1}{2}\right)^2\sigma_t^2-4\left(\frac{1}{4}+C_t^2\right)\left(\frac{\sigma_t^2}{4}+D_t^2\sigma_t^2-k^2\right)}}{2\left(\frac{1}{4}+C_t^2\right)},$$
$$\sigma_y(h_b)=\frac{-\left(2C_bD_b-\frac{1}{2}\right)\sigma_b+\sqrt{\left(2C_bD_b-\frac{1}{2}\right)^2\sigma_b^2-4\left(\frac{1}{4}+C_b^2\right)\left(\frac{\sigma_b^2}{4}+D_b^2\sigma_b^2-k^2\right)}}{2\left(\frac{1}{4}+C_b^2\right)}.$$

A.0.3 Derived Quantities

Due to the lack of assumptions on the physics away from the rollers, manifesting in the fact that from our inner model we do not know the whole stress tensor across the thickness, there are few quantities that we can derive from our model. It is straightforward to derive the pressure at the roll surfaces, since the $\sigma_x+\sigma_y$ yields twice the pressure (this follows from the fact that the deviatoric stress tensor is traceless). More interesting quantities to consider, considering that our ambient aim is a coupling with the outer model, are the horizontal and vertical forces, as well as the moments (anti-clockwise about the zero-line), across the roll gap.

$$F_h=\int_{h_b}^{h_t}\sigma_x\,dy=\Delta h\frac{\sigma_t+\sigma_b}{2},$$
$$F_v=\Delta h\,\overline{\tau},$$
$$M=-\int_{h_t}^{h_b}\sigma_x y\,dy=\Delta h\frac{-\sigma_t+\sigma_b}{2}.$$

A.1 Summary Of Equations

We now summarise all equations for the inner model relevant for the numerics.

A.1.1 Easing Notation

$$\rho_t=-2h_t^2+h_th_b+h_b^2$$
$$\rho_b=-2h_b^2+h_th_b+h_t^2$$
$$\mathrm{sgn_t}(x)=\mathrm{sgn}(x-x_t^n)\,\mathrm{hvsd}(x-x_t^{in})\,\mathrm{hvsd}(x_t^{out}-x)$$
$$\mathrm{sgn_b}(x)=\mathrm{sgn}(x-x_b^n)\,\mathrm{hvsd}(x-x_b^{in})\,\mathrm{hvsd}(x_b^{out}-x)$$

A.1.2 Reducing Degrees Of Freedom

$$
\begin{aligned}
C_t &= \frac{\mu \mathrm{sgn_t} - h_t'}{1 - h_t'^2 + 2\mu h_t' \mathrm{sgn_t}} \\
C_b &= \frac{-\mu \mathrm{sgn_b} - h_b'}{1 - h_b'^2 - 2\mu h_b' \mathrm{sgn_b}} \\
D_t &= \frac{\mu h_t'^2 \mathrm{sgn_t} + h_t'}{1 - h_t'^2 + 2\mu h_t' \mathrm{sgn_t}} \\
D_b &= \frac{-\mu h_b'^2 \mathrm{sgn_b} + h_b'}{1 - h_b'^2 - 2\mu h_b' \mathrm{sgn_b}} \\
\sigma_y(h_t) &= \frac{-\left(2C_tD_t - \frac{1}{2}\right)\sigma_t + \sqrt{\left(2C_tD_t - \frac{1}{2}\right)^2 \sigma_t^2 - 4\left(\frac{1}{4} + C_t^2\right)\left(\frac{\sigma_t^2}{4} + D_t^2\sigma_t^2 - k^2\right)}}{2\left(\frac{1}{4} + C_t^2\right)} \\
\sigma_y(h_b) &= \frac{-\left(2C_bD_b - \frac{1}{2}\right)\sigma_b + \sqrt{\left(2C_bD_b - \frac{1}{2}\right)^2 \sigma_b^2 - 4\left(\frac{1}{4} + C_b^2\right)\left(\frac{\sigma_b^2}{4} + D_b^2\sigma_b^2 - k^2\right)}}{2\left(\frac{1}{4} + C_b^2\right)} \\
\tau_t &= C_t\sigma_y + D_t\sigma_t \\
\tau_b &= C_b\sigma_y + D_b\sigma_b
\end{aligned}
$$

A.1.3 Differential Equations

$$
\begin{aligned}
\partial_x\sigma_b &= \frac{6}{\rho_b}\left(\Delta h\,\overline{\tau} - h_t\tau_t + h_b\tau_b\right) + \left(-\frac{\rho_t}{\rho_b}\,\sigma_t + \sigma_b\right)\frac{1}{\Delta h}\frac{d\Delta h}{dx} - \frac{3(\sigma_b h_t' - \sigma_t h_b')(h_t + h_b)}{\rho_b} + \frac{\rho_t}{\rho_b}\,\partial_x\sigma_t \\
\partial_x\overline{\tau} &= \frac{1}{\Delta h}\left(h_t'\tau_t - \sigma_y(h_t) - h_b'\tau_b + \sigma_y(h_b) - \overline{\tau}\frac{d\Delta h}{dx}\right) \\
\partial_x\sigma_t &= \frac{2}{\Delta h}(-\tau_t + \tau_b - h_t'\sigma_b + h_b'\sigma_t) + \frac{\sigma_t + \sigma_b}{\Delta h}\frac{d\Delta h}{dx} - \partial_x\sigma_b
\end{aligned}
$$

A.1.4 Derived Quantities

$$
\begin{aligned}
F_h &= \int_{h_b}^{h_t} \sigma_x\,dy = \Delta h\frac{\sigma_t + \sigma_b}{2}, \\
F_v &= \Delta h\,\overline{\tau}, \\
M &= -\int_{h_t}^{h_b} \sigma_x y\,dy = \Delta h\frac{-\sigma_t + \sigma_b}{2}.
\end{aligned}
$$

B Numerics

For users of our package, the master file which synthesises all inner and outer model code in *pproc.m*. In this *m*-file, the function *inner_model* yields the horizontal stress and average shear stress data across the roll gap. These are then post-processed to obtain horizontal and vertical forces, as well

as moments. The data is then plotted against the displacement across the roll gap. The function *plotdisplacements* then plots a ring profile subject to the forces and moments obtained at the end of the roll gap. The geometry of the model is encoded in the function *initGeom*. In order to change the model, these functions - and their associated files - should be changed; it should not be necessary to change much in the master file *pproc.m*, except material properties and some outer model simplifications. The datasets, contained in *run.m*, are then fully specified by created a struct in MATLAB that contains the following variables[12]:

- w_0 - Minimum point of separation of the rolls;
- R_t- Radius of the top roll;
- R_b- Radius of the bottom roll;
- $entry_t$ - Roll gap entry point at the top;
- $entry_b$ - Roll gap entry point at the bottom;
- $exit_b$ - Roll gap exit point at the top;
- $neut_t$ - Roll gap neutral point at the top;
- $neut_b$ - Roll gap neutral point at the bottom;
- *name* - Name of rolling configuration.

The material properties that have to be specified in *pproc.m*[13] are:

- *mu* - The coefficient of friction;
- k - The yield stress;
- E - Young's modulus;
- G - Shear modulus.

B.1 Numerical Data

[12]The labels for these variables are those used in the MATLAB code. They do not always agree with the labels we have used in this report, but we hope it is clear when there is disagreement.

[13]Material properties should not have to be in this file, and this can be achieved by using parent classes in *run.m*. We hold these fixed throughout our testing, so this is why we decided not to do this.

Figure 6: Flat, Symmetric, Thin-Sheet Rolling

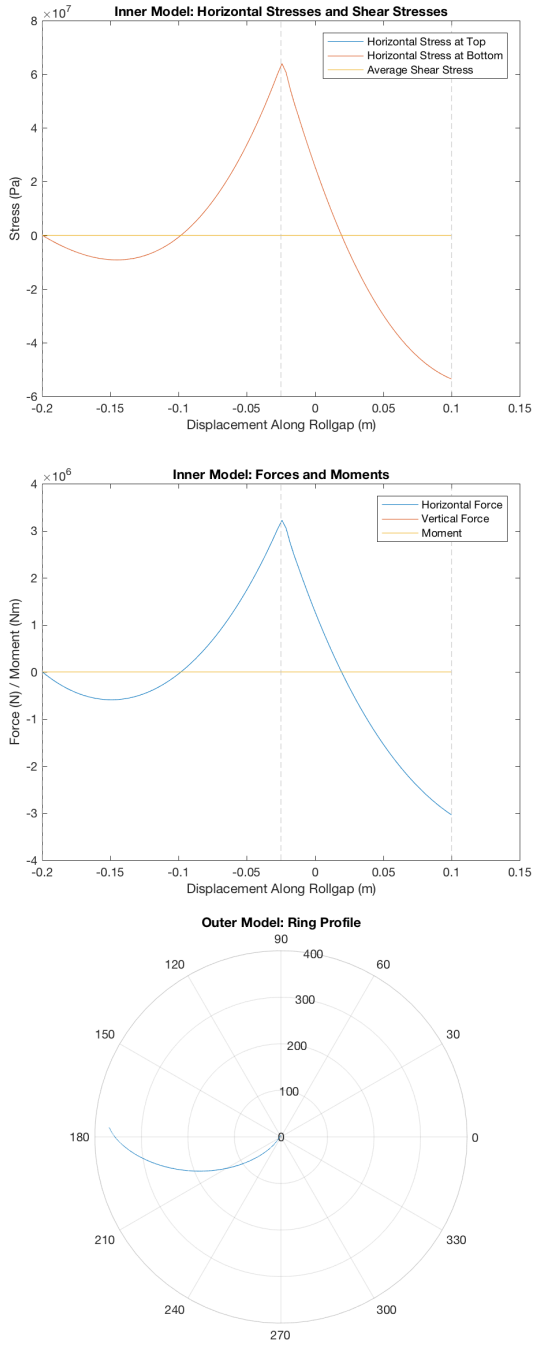

Figure 7: Flat, Symmetric, Thick-Sheet Rolling

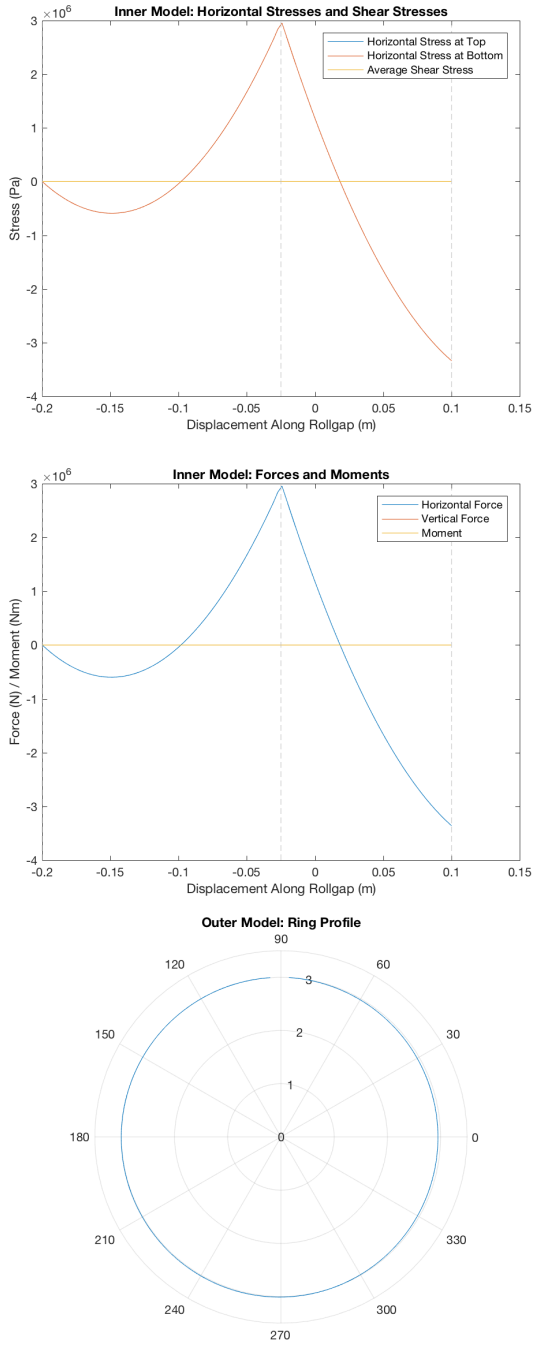

Figure 8: Curved, Symmetric Rolling

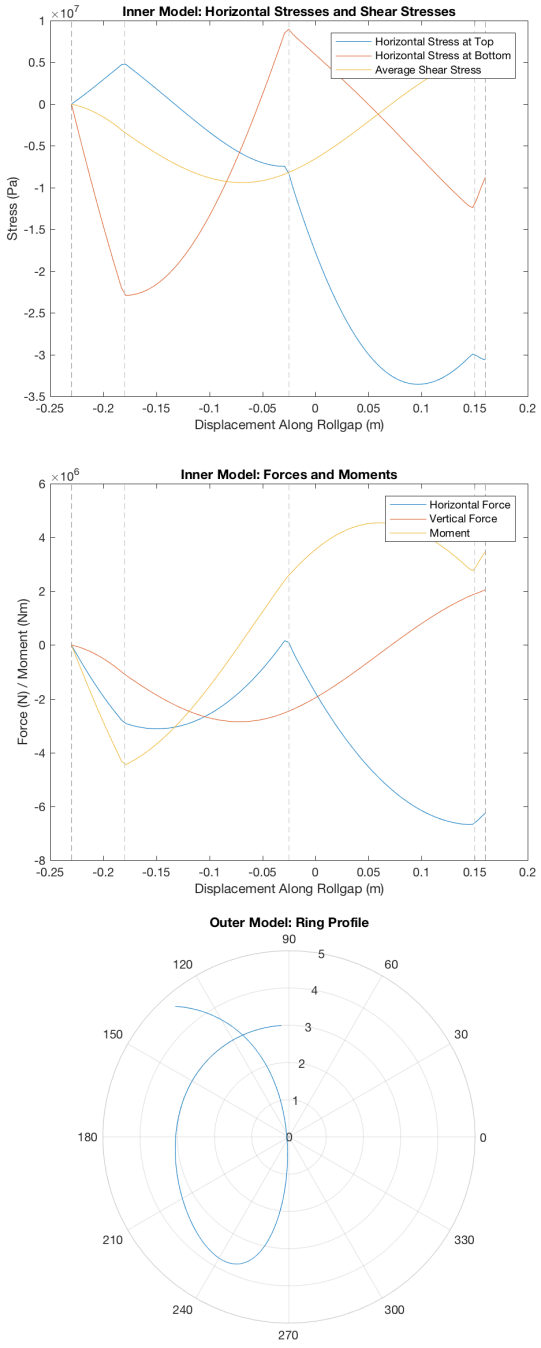

Figure 9: Curved, Asymmetric Rolling

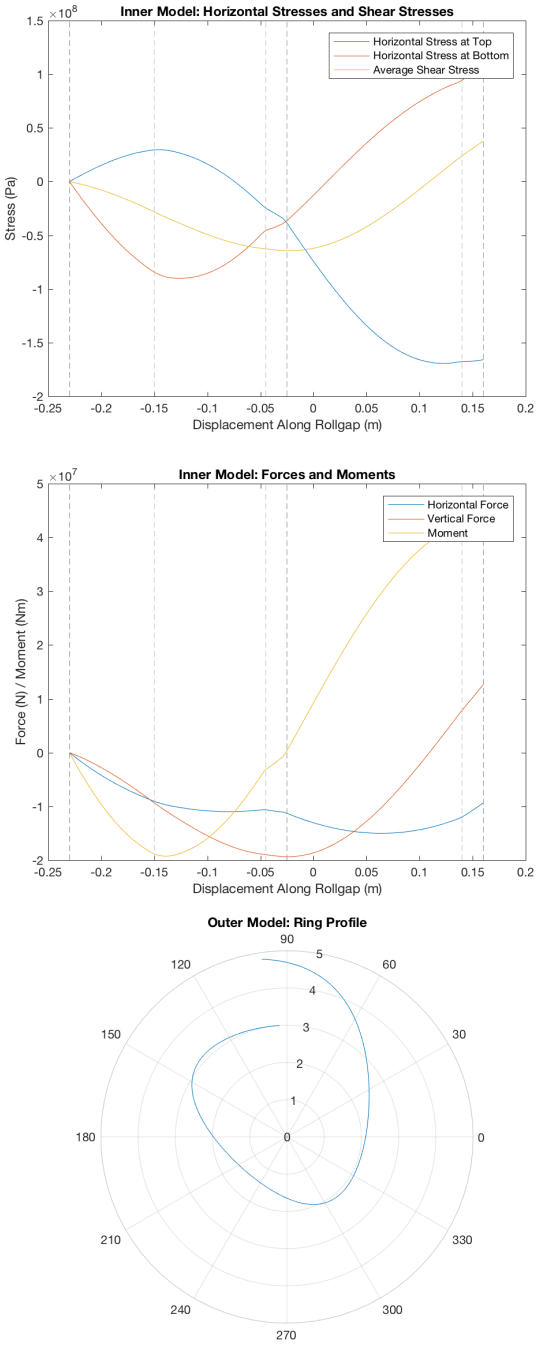

Figure 10: Very Small Aspect Ratio

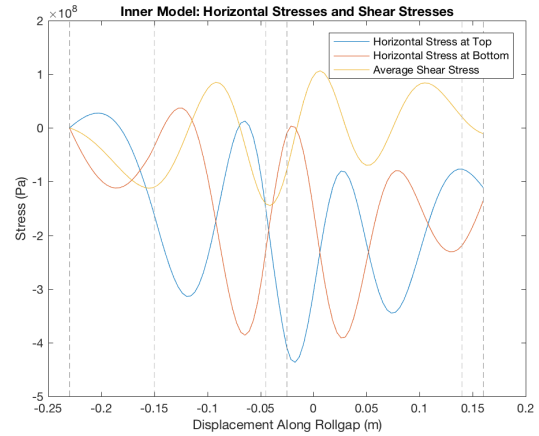

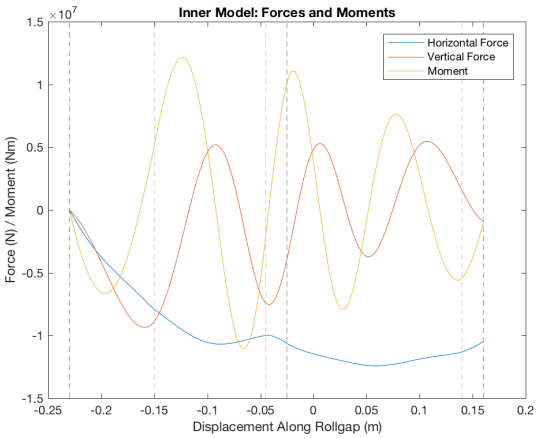

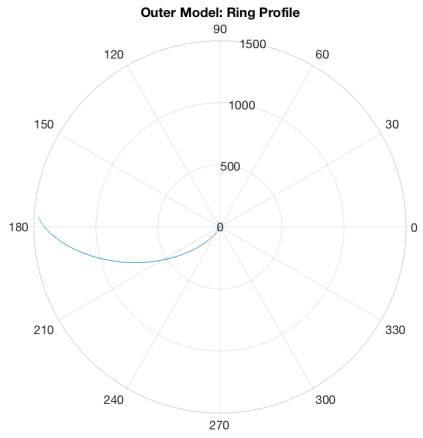

Figure 11: Small Aspect Ratio

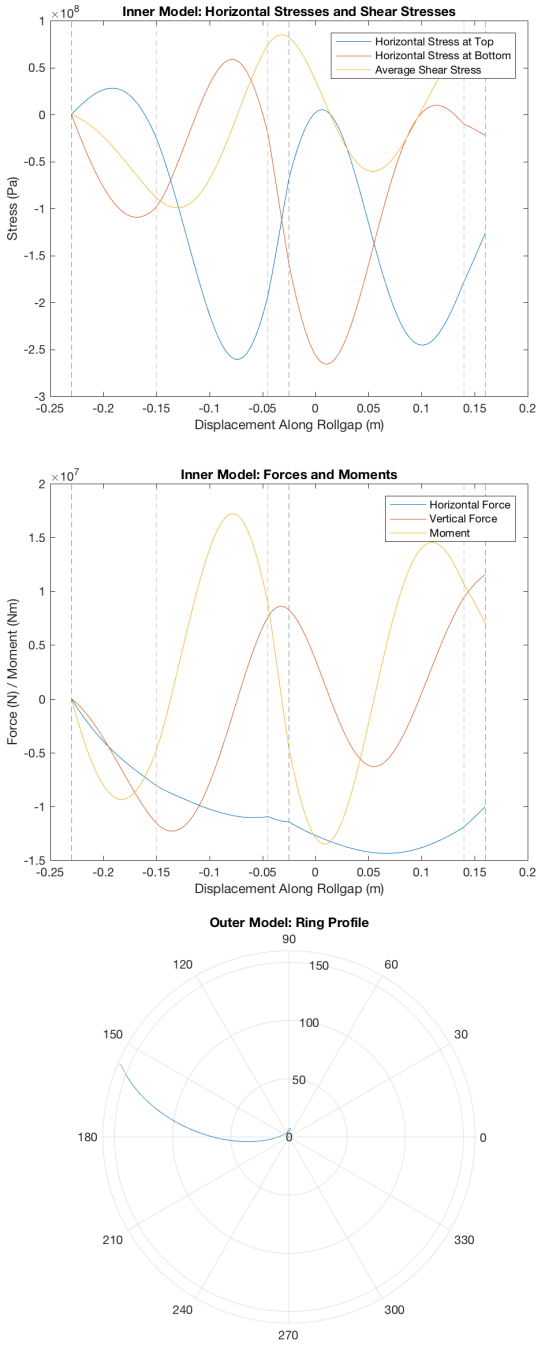

Figure 12: Moderate Aspect Ratio

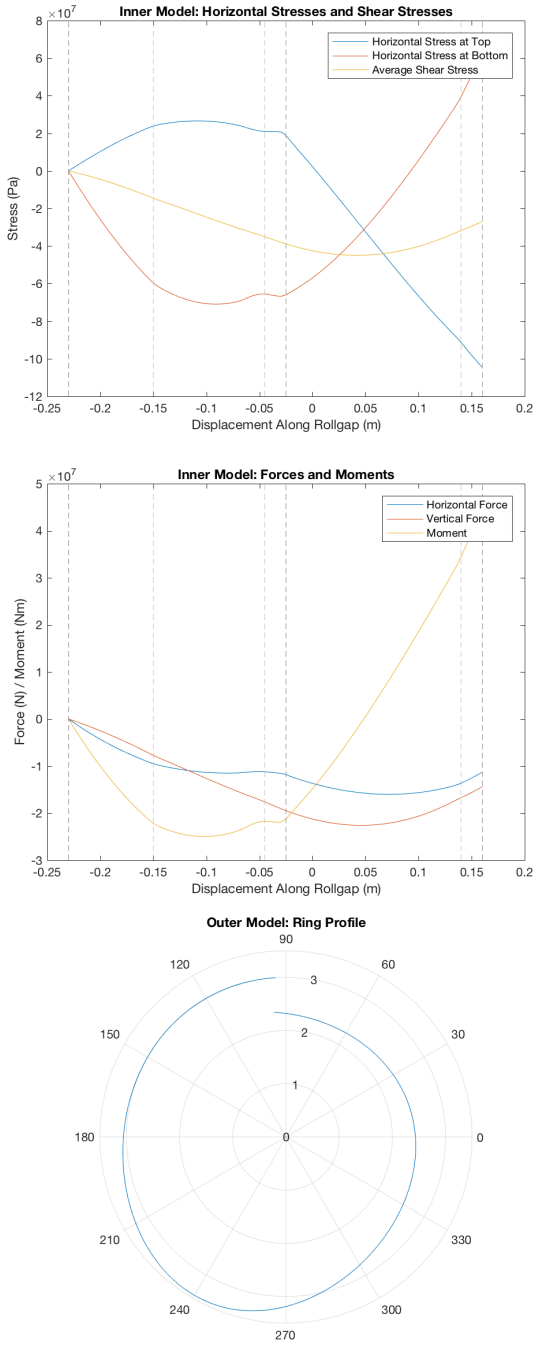

Figure 13: Large Aspect Ratio

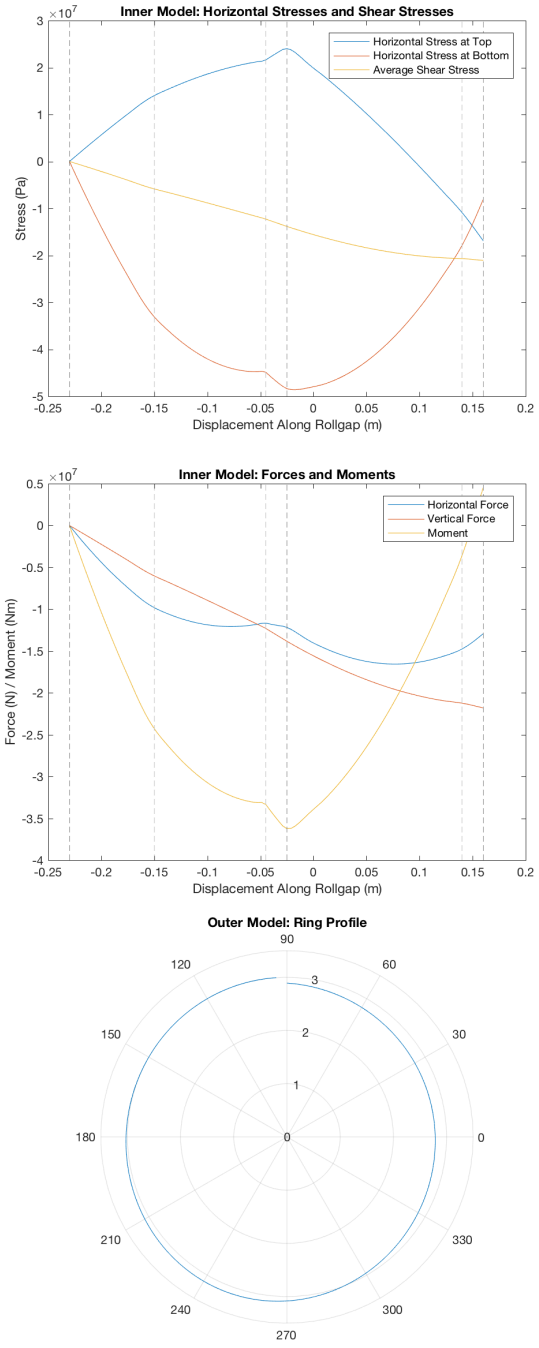

B.1.1 Rolling Configurations

Figure 6: $w_0 = 0.05$, $R_t = 1.5$, $R_b = 1.5$, $entry_t = -0.2$, $entry_b = -0.2$, $exit_t = 0.1$, $exit_b = 0.1$, $neut_t = -0.025$, $neut_b = -0.025$.
Figure 7: $w_0 = 1$, $R_t = 1.5$, $R_b = 1.5$, $entry_t = -0.2$, $entry_b = -0.2$, $exit_t = 0.1$, $exit_b = 0.1$, $neut_t = -0.025$, $neut_b = -0.025$.
Figure 8: $w_0 = 0.3$, $R_t = 1.5$, $R_b = 1.5$, $entry_t = -0.23$, $entry_b = -0.18$, $exit_t = 0.16$, $exit_b = 0.15$, $neut_t = -0.025$, $neut_b = -0.025$.
Figure 9: $w_0 = 0.3$, $R_t = 1.5$, $R_b = 0.5$, $entry_t = -0.23$, $entry_b = -0.15$, $exit_t = 0.16$, $exit_b = 0.14$, $neut_t = -0.025$, $neut_b = -0.045$.
Figure 10: $w_0 = 0.05$, $R_t = 1.5$, $R_b = 0.5$, $entry_t = -0.23$, $entry_b = -0.15$, $exit_t = 0.16$, $exit_b = 0.14$, $neut_t = -0.025$, $neut_b = -0.045$.
Figure 11: $w_0 = 0.1$, $R_t = 1.5$, $R_b = 0.5$, $entry_t = -0.23$, $entry_b = -0.15$, $exit_t = 0.16$, $exit_b = 0.14$, $neut_t = -0.025$, $neut_b = -0.045$.
Figure 12: $w_0 = 0.5$, $R_t = 1.5$, $R_b = 0.5$, $entry_t = -0.23$, $entry_b = -0.15$, $exit_t = 0.16$, $exit_b = 0.14$, $neut_t = -0.025$, $neut_b = -0.045$.
Figure 13: $w_0 = 1$, $R_t = 1.5$, $R_b = 0.5$, $entry_t = -0.23$, $entry_b = -0.15$, $exit_t = 0.16$, $exit_b = 0.14$, $neut_t = -0.025$, $neut_b = -0.045$.

References

[AAA16] A Aboutorabi, A Assempour, and H Afrasiab. Analytical approach for calculating the sheet output curvature in asymmetrical rolling: In the case of roll axis displacement as a new asymmetry factor. *International Journal of Mechanical Sciences*, 105:11–22, 2016.

[BQM15] GA Berti, Luca Quagliato, and Manuel Monti. Set-up of radial–axial ring-rolling process: Process worksheet and ring geometry expansion prediction. *International Journal of Mechanical Sciences*, 99:58–71, 2015.

[GY11] Lianggang Guo and He Yang. Towards a steady forming condition for radial–axial ring rolling. *International Journal of Mechanical Sciences*, 53(4):286–299, 2011.

[HJKA73] JB Hawkyard, W Johnson, J Kirkland, and E Appleton. Analyses for roll force and torque in ring rolling, with some supporting experiments. *International Journal of Mechanical Sciences*, 15(11):873–893, 1973.

[KMK90] Naksoo Kim, Susumu Machida, and Shiro Kobayashi. Ring rolling process simulation by the three dimensional finite element method. *International Journal of Machine Tools and Manufacture*, 30(4):569–577, 1990.

[Lub08] Jacob Lubliner. *Plasticity theory*. Courier Corporation, 2008.

[MH94] Jerrold E. Marsden and Thomas J. R. Hughes. *Mathematical foundations of elasticity*. Dover Publications, Inc., New York, 1994. Corrected reprint of the 1983 original.

[Min17] Jeremy J. Minton. Mathematical modelling of asymmetrical metal rolling processes, 2017. PhD thesis, University of Cambridge.

[PA14] A Parvizi and K Abrinia. A two dimensional upper bound analysis of the ring rolling process with experimental and fem verifications. *International Journal of Mechanical Sciences*, 79:176–181, 2014.

[PAS11] A Parvizi, K Abrinia, and M Salimi. Slab analysis of ring rolling assuming constant shear friction. *Journal of materials engineering and performance*, 20(9):1505–1511, 2011.

[RDS17] NA Razani, B Mollaei Dariani, and M Soltanpour. Analytical approach of asymmetrical thermomechanical rolling by slab method. *The International Journal of Advanced Manufacturing Technology*, pages 1–15, 2017.

[Sha64] Irving Herman Shames. *Mechanics of deformable solids*. Prentice-Hall, 1964.

[TG51] S. Timoshenko and J. N. Goodier. *Theory of Elasticity*. McGraw-Hill Book Company, Inc., New York, Toronto, London, 1951. 2d ed.

[Tim25] Stephen Timoshenko. *Applied elasticity*. Westinghouse Tech. Night Press, 1925.

[TIST05] Kazuhito TANI, Shinya ISHIGAI, Takao SATO, and Yoshikatsu TSUMORI. The evolution of near-net-shape ring-rolling processes for large rings made of ti-6al-4v. *R & D Kōbe Seikō gihō*, 55(2):51–55, 2005.

[YKKL03] Youngsoo Yea, Youngsoo Ko, Naksoo Kim, and Jongchan Lee. Prediction of spread, pressure distribution and roll force in ring rolling process using rigid–plastic finite element method. *Journal of materials processing technology*, 140(1):478–486, 2003.